

## Statistical mechanics of bilayer membrane with a fixed projected area

O. Farago<sup>1,2</sup>, and P. Pincus<sup>1,2</sup><sup>1</sup> Materials Research Laboratory, University of California, Santa Barbara, CA 93106<sup>2</sup> Department of Physics, Korea Advanced Institute of Science and Technology (KAIST),  
373-1 Kusong-dong, Yuseong-gu, Taejeon 305-701, South Korea.

(Dated: March 22, 2024)

The equilibrium and fluctuation methods for determining the surface tension,  $\gamma$ , and bending modulus,  $\kappa$ , of a bilayer membrane with a fixed projected area are discussed. In the fluctuation method the elastic coefficients  $\gamma$  and  $\kappa$  are measured from the amplitude of thermal fluctuations of the planar membrane, while in the equilibrium method the free energy required to deform the membrane is considered. The latter approach is used to derive new expressions for  $\gamma$  and  $\kappa$  (as well as for the saddle-splay modulus), which relate them to the pair-interactions between the amphiphiles forming the membrane. We use linear response theory to argue that the two routes lead to similar values for  $\gamma$  and  $\kappa$ . This argument is confirmed by Monte Carlo simulations of a model membrane whose elastic coefficients are calculated using both methods.

PACS numbers:

Electronic address: farago@mrl.ucsb.edu

## I. INTRODUCTION

The Bilayer membrane, a double sheet of surfactants separating two aqueous phases, is one of the structures formed by the self-assembly of amphiphilic molecules in water [1]. The driving force in this process is the hydrophobic effect which favors exposing the hydrophilic part of the molecules to the water while shielding the "oily" part from aqueous contact [2, 3]. The ongoing interest in such membranes is due to many reasons, among which are their predominant role in the organization of the biological cells [4], and their various applications in many industrial sectors [5]. Bilayer amphiphilic sheets have very special mechanical properties: While being strongly resistant to lateral mechanical stretching or compression, they are highly flexible and can exhibit large thermally excited undulations [6, 7]. This unique elastic behavior, namely the stability against external perturbations on the one hand, but the ease in going from one shape to another on the other hand, is important for the activity of living cells [8]. Consequently, there has been a great effort to understand the elasticity of bilayer systems [6, 7, 9, 10].

Bilayer membranes are quasitwo-dimensional (2D) objects: their thickness is typically of the size of a few nanometers (roughly, twice the length of the constituent amphiphilic molecules), while their lateral extension can reach up to several micrometers. Since the membrane appears as a thin film on the mesoscopic scale, its physical properties are often studied using coarse-grained phenomenological models treating the membrane as a smooth continuous 2D sheet [6, 7, 9, 11]. Membrane elasticity has been traditionally studied using the Helfrich effective surface Hamiltonian which relates the elastic energy to the local principle curvatures of the membrane  $c_1$  and  $c_2$ , and which has the following form [12]:

$$H = \int_A dS \left[ \gamma_0 + \frac{1}{2} \gamma_0 (J - 2c_0)^2 + \gamma_0 K \right]; \quad (1)$$

where  $J = c_1 + c_2$  and  $K = c_1 c_2$  are the total and Gaussian curvatures respectively. The integration in Eq.(1) is carried over the whole surface of the membrane. The Helfrich Hamiltonian is derived by assuming that local curvatures are small, and the free energy can be expanded to second order in  $J$  and to first order in  $K$ . It, therefore, involves four phenomenological parameters: the spontaneous curvature  $c_0$ , and three elastic coefficients—the surface tension  $\gamma_0$ , the bending modulus  $\gamma_0$ , and the saddle-splay modulus  $\gamma_0$ , whose values depend on the area density of the amphiphiles. If the number of these is fixed, then one should also consider the corrections to Hamiltonian (1) due to the changes in the area of the fluctuating membrane. For weakly fluctuating membranes these corrections can be assumed to be small. The surface tension, which is usually associated with the free energy cost for adding molecules to the membrane (at a fixed density), is related in the case of membranes with fixed number of amphiphiles to the area-density dependent (Schulman) elastic energy [13, 14, 15].

The Helfrich Hamiltonian has been very successful in describing the shape and the phase diagram of complex interfaces [16, 17, 18]. It also yields a correct description of the thermal fluctuations around the equilibrium surface state [19, 20, 21], and of the entropic forces between membranes [22]. Because it is phenomenological, the Helfrich Hamiltonian provides no information about the values of the elastic coefficients. Many theories have been developed that attempt to relate the elastic coefficients introduced by the Helfrich Hamiltonian to microscopic entities and the interactions between them [23, 24, 25, 26, 27]. In fact, these theories are usually concerned with the free energy of the surface, rather than the Hamiltonian. The free energy is assumed to have the same form as the Helfrich Hamiltonian and, hence, usually called the Helfrich free energy (see a more detailed discussion in section II). The coefficients appearing in the expression for the free energy, which we denote by  $\gamma$ ,  $\kappa$ , and  $\bar{\kappa}$ , are also referred to as the surface tension, the bending modulus, and the saddle-splay modulus, respectively. Despite the similarity in names, there is a significant difference between the Hamiltonian coefficients (with the subscript 0) and the free energy coefficients. The former are "material properties" which depend on the internal (potential) energy of the surface. The latter, on the other hand, are thermodynamic quantities and, as such, are also influenced by the entropy associated with the thermal fluctuations of the system. Their values, therefore, may also depend on the temperature and the size of the system.

In addition to the above mentioned theories, there has been also an effort to analyze the elastic behavior in the context of the thermodynamics and statistical mechanics of curved interfaces [28, 29, 30, 31, 32, 33]. The last approach has the potential of providing exact "virial" expressions for  $\gamma$ ,  $\kappa$ , and  $\bar{\kappa}$  in terms of the microscopic forces between the amphiphiles and the pair distribution function. One of the systems whose statistical mechanics has been studied extensively is that of a simple liquid-vapor interface. Although this seems to be a rather simple system, the determination of its elastic moduli is quite complicated and involves a set of technical and conceptual problems. Below we discuss some of them:

One problem is related to the finite thickness of the interface, namely to the fact that the local concentration is not a step function but changes gradually while going from one phase to the other. Consequently, there is some ambiguity about the location of the dividing plane that separates the two phases and to which the Helfrich Hamiltonian is applied. It turns out that the values of the rigidity constants  $\kappa$  and  $\bar{\kappa}$  (the coefficients of the second order terms in the curvatures  $c_1$  and  $c_2$ ) depend on the choice of the dividing surface [34]. The dependence of the rigidity constants on the reference surface had led people to question the validity of continuing the Helfrich free energy expansion beyond the linear term in curvature. This problem has been recently tackled by van Giessen and Blokhuis [35] who used computer simulation to determine the rigidity constants of a curved liquid-vapor interface in a system of particles interacting via a truncated Lennard-Jones (LJ) potential. They have demonstrated that although one needs to state which convention for locating the dividing surface is used when providing the values of  $\kappa$  and  $\bar{\kappa}$ , this fact does not render the Helfrich free energy useless, nor does it diminish the importance of these quantities in describing the elastic properties of the interface.

A second problem that makes the determination of the rigidity constants difficult is a technical one: In their paper van Giessen and Blokhuis used the virial expressions given in Ref. [36] to evaluate the values of  $\kappa$  and  $\bar{\kappa}$ . These expressions relate the rigidity constants to the derivative of the pair density distribution function with respect to the radius of curvature  $R_c$ . This means that the values of the rigidity constants of a planar interface cannot be determined from the simulation of that system only, but it is necessary to perform a set of simulations of curved interfaces with very large values of  $R_c$ . For the interfaces investigated in Ref. [35], it turns out that in the large  $R_c$  regime the dependence of the pair density function on  $R_c$  is very weak. Consequently, it was impossible to determine  $\kappa$  and  $\bar{\kappa}$  accurately, and only a rough estimate of these quantities could be obtained.

A third problem, a more fundamental one, is related to the method of calculating the rigidity constants  $\kappa$  and  $\bar{\kappa}$  and to our interpretation of their physical meaning. The theoretical and experimental methods for determining the elastic coefficients of interfaces can be classified into equilibrium (or mechanical) methods and fluctuation methods [37, 38]. The difference between these two approaches is in the context in which the Helfrich Hamiltonian and the associated free energy are used: In the equilibrium approach one extracts the elastic coefficients by comparing the free energies of two equilibrium surfaces with different curvatures. In the fluctuation approach, on the other hand, the Helfrich Hamiltonian is used to calculate the free energy cost due to a thermal fluctuation that changes the local curvature from its equilibrium value. The elastic coefficients are derived from the mean-square amplitudes of the fluctuations. The situation in which there exist two methods for calculating elastic moduli is reminiscent of other cases, for instance, the two different methods of evaluating the elastic constants of thermodynamic systems in linear elasticity theory [39, 40, 41, 42], and the two approaches for determining the surface tension of a planar interface [43, 44]. In the latter examples the different approaches lead to the same values for the mechanical moduli, in accord with the linear response theory [45, 46]. This is not the case with the rigidity constants of a liquid-vapor interface [37]. The discrepancy between the two methods

is due to the fact that in order to change the equilibrium radius of curvature of, say, a spherical liquid drop, it is necessary to change its volume as well. This means a change in the volume fractions of the two phases (i.e., the condensation of vapor or the evaporation of liquid), and it thus requires the variation of the thermodynamic variables like the temperature or the chemical potential. In the fluctuation case the radius of curvature is varied by thermal fluctuations, while the thermodynamic variables are not altered.

In this paper we discuss the statistical mechanics of fluid bilayer membranes. We derive expressions for the elastic coefficients  $\gamma$ ,  $\kappa$ , and  $\bar{\kappa}$  of the membranes, relating them to the interactions and the correlation functions between the amphiphiles forming the bilayer. We use these expressions for a Monte Carlo (MC) determination of the elastic coefficients of a bilayer membrane computer model. Unlike the expressions derived for the rigidity constants of a liquid-vapor interface, our expressions are such that they can be evaluated using a single MC run performed on the (quasi) flat membrane reference system only. This feature greatly simplifies the computational procedure, and makes it more efficient and well-controlled. Another important distinction between the membranes discussed in this paper and the system of liquid-vapor interface studied in Ref. [35] is the fact that the mechanical and the fluctuation methods for determining their rigidity constants lead to similar results. Our expressions are derived using the mechanical approach, namely by calculating the free energy variations resulting from the change in the area and curvature of the membrane. The numerical values of the elastic coefficients which we obtain from these expressions are compared with the values extracted from a spectral analysis of the thermal fluctuations around the flat reference state. We find a very good agreement between the two methods. This agreement, which is expected by virtue of linear response theory (see discussion in section II), reflects the fact that the curvature of the membrane can be varied by changing the shape of the container (namely, by the application of external forces) without affecting the thermodynamic properties of the bulk aqueous phases surrounding it. It should be noted that the experimental values of  $\gamma$  measured (for the same lipid bilayers) using mechanical and fluctuation methods can differ by as much as a factor of 3 [38]. The origin of these discrepancies is not well understood.

The bilayer computer model which we use in this paper has been recently introduced by one of us [47]. (Here we use a slightly modified version of that model which we describe in section IV.) This model has two features which simplify the derivation of thermodynamic expressions for the elastic coefficients and the simulations performed for the calculation of these expressions. First, the simulations are conducted with no solvent present in the simulation cell, i.e., as if the membrane is in vacuum. This feature greatly reduces the number of atoms in the simulation cell, thus enabling us to simulate a relatively large membrane over a very long MC run. The ability to perform long MC runs is very important since the quantities whose thermal averages we try to evaluate are very "noisy", and accurate results can be obtained only if they are measured for a large number of configurations. The other feature is the nature of the interactions between the molecules forming the membrane. In our computer model the amphiphilic molecules are modeled as trimers and the interactions between their constituent atoms are pairwise additive. For such systems the derivation of expression for the elastic coefficients (see section III) is simpler than for systems including many-body potentials. Our discussion in this paper is, therefore, restricted to central force systems only.

The paper is organized in the following way: The theoretical aspects of our study are presented in sections II and III. In section II we describe the relation between the equilibrium and the fluctuation routes for determining the surface tension and the bending modulus of bilayer membranes, and explain why these methods (if used appropriately) lead to similar results. Then, in section III, we derive expressions for these quantities based on the equilibrium approach. Our expressions relate  $\gamma$  and  $\kappa$  to the interactions and the correlation functions between the "interaction sites" of the amphiphilic molecules. The numerical results are presented in section IV where we calculate the elastic coefficients of our model system using the two methods and find a very good agreement between them. Some technical aspects of the simulations are discussed in the Appendix. Finally we conclude in section V.

## II. THE EQUILIBRIUM AND FLUCTUATION ROUTES TO MEMBRANE ELASTICITY

Linear response is a fundamental theorem which relates the fluctuations of a system around its equilibrium state and the response of the system to weak perturbations [45, 46]. In the context of elasticity theory it provides a link between the shape fluctuations of thermodynamic systems and their elastic moduli. For example, when a 2D flat interface is slightly stretched or compressed from its equilibrium area  $A_0$ , the variation of the (small) surface pressure is given by [48, 49]

$$K_A = -A_0 \frac{\partial \gamma}{\partial A}; \quad (2)$$

where  $A$  is the area of the interface and  $K_A$  is the stretching/compression modulus. The above relation provides one way to measure  $K_A$ . An alternative approach for measuring  $K_A$  is to consider the thermal fluctuations of the area  $A$

around the equilibrium area  $A_0$  [40, 50]. The equipartition theorem suggests that in the low temperature limit when fluctuations around  $A_0$  are small

$$\langle (A - A_0)^2 \rangle = \frac{k_B T A}{K_A}; \quad (3)$$

where  $k_B$  is the Boltzmann constant and  $T$  is the temperature, while  $\langle \dots \rangle$  denotes a thermal average. Linear response theory can be also applied to describe the normal, curvature-forming, fluctuations of the 2D interface. The discussion in this case (of normal fluctuations) is, however, somewhat more complicated. A proof of the equivalence between the equilibrium and the fluctuation routes to the surface tension of a fluctuating interface had been presented with great clarity by Cai et al. [51]. Below we extend that proof and address the two routes to the bending modulus as well. One important difference between the present discussion and the one presented in Ref. [51] is related to the nature of the fluctuating surfaces in question. Here, we consider an elastic surface consisting of a fixed number of molecules whose area density is varied when it fluctuates. By contrast, the surface studied in Ref. [51] is incompressible and its area density is fixed to its equilibrium value. The variation of the total area of the latter is achieved via the exchange of molecules between the surface and the embedding solvent. A more detailed discussion on the differences between the elastic properties of compressible and incompressible surfaces appears in Ref. [15].

Let us consider a 2D surface that spans a planar frame of a total area  $A_p$  which does not necessarily coincide with the equilibrium (Schulman) area  $A_0$ . The surface is free to undulate in the direction normal to frame. The ensemble of conformations which the surface attains is governed by a Hamiltonian  $H(h(\mathbf{r}))$  relating the elastic energy to the conformation of the surface. The conformation of the surface is described by some "gauge" function  $h(\mathbf{r})$ , where  $\mathbf{r} = (x, y)$  label the points on the reference surface. The exact form of the Hamiltonian  $H$  is unimportant and, in particular, it is not limited to the Helfrich form (1). As we are interested in moderately-fluctuating surfaces (with no overhangs), we shall use the so called Monge gauge  $z = h(\mathbf{r})$ , where  $h$  is the height of the surface above the frame reference plane. In what follows we will restrict our discussion to symmetric surfaces (such as bilayers) with no spontaneous curvature, i.e., with no preference to bend toward either the "upper" or "lower" side of the surface. In other words, we assume that the average conformation of the surface is flat and for each  $\mathbf{r}$

$$\langle h(\mathbf{r}) \rangle = 0; \quad (4)$$

We also assume that the surface under consideration is mechanically stable, and that the validity of Eq.(4) is not due to the partition of the configurations phase space into several sub spaces for which  $\langle h(\mathbf{r}) \rangle \neq 0$ .

If the frame (projected) area  $A_p$  is not equal to the equilibrium area  $A_0$  then it is necessary to apply a tangential surface pressure in order to fix the area of the frame. If, in addition, normal forces are applied then relation (4) breaks down. The function

$$h(\mathbf{r}) = \langle h(\mathbf{r}) \rangle \quad (5)$$

can be regarded as the strain field describing the deformed state of the surface. The free energy of a system subjected to a small deformation can be expanded in a power series in the strain variables. In full analogy to Hamiltonian (1), we can write the Helfrich free energy of the surface in the following form :

$$F[h] = F[h=0] + \int_{A_p} d\mathbf{r} \left( \frac{1}{2} J^2 h^2 + K h + \dots \right); \quad (6)$$

where  $\int_{A_p} d\mathbf{r}$  is total area of the surface defined by the function  $h(\mathbf{r})$ , while  $J^2$  and  $K$  denote, respectively, the integrated total and Gaussian curvatures defined by

$$J^2 = \int_{A_p} d\mathbf{r} J^2 h(\mathbf{r}); \quad (7)$$

and

$$K = \int_{A_p} d\mathbf{r} K h(\mathbf{r}); \quad (8)$$

In Eq.(6) we set the spontaneous curvature  $c_0 = 0$  [see Eqs.(4) and (5)], and use the effective (normalized) values of the elastic coefficients which are different from the "bare" values appearing in the Hamiltonian (1) (see discussion earlier in section I). The higher order terms (h.o.t) in Eq.(6) include both products of the small variables  $(A - A_p) = A_p$ ,  $J^2$ , and  $K$ , as well as terms involving the gradients of the local curvatures. The latter are assumed to be small since we consider only nearly-flat surfaces described by functions  $h$  which vary slowly in space. Since  $\nabla^2 h$ ,  $\nabla^4 h$ , and  $\nabla^6 h$  appear

as the coefficients of the free energy expansion in strain variables [Eq.(6)], they can be also related to the following partial derivatives

$$= \frac{\partial F}{\partial A} \bigg|_{h(\mathbf{r})=0}; \quad (9)$$

$$= \frac{\partial^2 F}{\partial J^2} \bigg|_{h(\mathbf{r})=0}; \quad (10)$$

and

$$= \frac{\partial F}{\partial K} \bigg|_{h(\mathbf{r})=0}; \quad (11)$$

evaluated at the reference state  $h(\mathbf{r}) = 0$ .

Equations (9)-(11) express the equilibrium (mechanical) route to  $\gamma$ ,  $\kappa$ , and  $\chi$ . The complementary fluctuations approach is more easily formulated in Fourier rather than in real space. Let us take a square frame (the reference surface) of linear size  $L_p = \sqrt{A_p}$ , and discretized it into  $N^2$  square cells ("patches") of linear size  $l = L_p/N$ , where  $l$  is some microscopic length of the order of the size of the constituent molecules. Since the description of the membrane as a 2D continuous sheet breaks down on length scales below  $l$ , the surface has to be defined only over a discrete set of points  $\mathbf{r}_g = (x_g, y_g)$  each of which located in the center of a grid cell. Outside the frame region, the function can be defined by periodic extension of period  $L_p$ , i.e.  $h(x_g + n_1 L_p, y_g + n_2 L_p) = h(x_g, y_g)$  where  $n_1$  and  $n_2$  are integer numbers. The Fourier transform of the (real) function  $h(\mathbf{r}_g)$  is defined by

$$h_{\mathbf{q}} = \frac{1}{L_p} \sum_{\mathbf{r}_g} h(\mathbf{r}_g) e^{i\mathbf{q} \cdot \mathbf{r}_g}; \quad (12)$$

where the two dimensional wave-vector  $\mathbf{q}$  has  $N^2$  discrete values satisfying

$$q_x, q_y = 2\pi m/L_p; m = 0, \pm 1, \pm 2, \dots, \pm N/2 - 1; \quad (13)$$

The inverse transform is given by

$$h(\mathbf{r}_g) = \frac{1}{L_p} \sum_{\mathbf{q}} h_{\mathbf{q}} e^{i\mathbf{q} \cdot \mathbf{r}_g}; \quad (14)$$

If the topology of the surface is fixed and it does not form "handles" then the periodicity of the surface leads to the vanishing of the Gaussian curvature (8) (Gauss-Bonnet theorem). Writing the expressions for the area  $A_h$  and the integrated total curvature  $J$  in terms of Fourier coordinates:

$$A_h = A_p + \frac{l^2}{2} \sum_{\mathbf{q}} q^2 h_{\mathbf{q}} h_{-\mathbf{q}} + O(l^4 h_{\mathbf{q}}^4) \quad (15)$$

and

$$J^2 h = l^2 \sum_{\mathbf{q}} q^4 h_{\mathbf{q}} h_{-\mathbf{q}} + O(l^4 h_{\mathbf{q}}^4); \quad (16)$$

and substituting them in Eq.(6), we obtain the following expression for the free energy

$$F_h = F_h = 0 + \frac{l^2}{2} \sum_{\mathbf{q}} (q^2 + q^4 + O(q^6)) h_{\mathbf{q}} h_{-\mathbf{q}} + O(l^4 h_{\mathbf{q}}^4); \quad (17)$$

The free energy (17) can be related to the surface Hamiltonian  $H(h(\mathbf{r}_g))$  via the partition function. We may use the Fourier transform

$$h_{\mathbf{q}} = \frac{1}{L_p} \sum_{\mathbf{r}_g} h(\mathbf{r}_g) e^{i\mathbf{q} \cdot \mathbf{r}_g} \quad (18)$$

of the function  $h(\mathbf{f}_{\mathbf{q}}g)$ , and express the Hamiltonian as a function of the Fourier modes:  $H(\mathbf{f}_{\mathbf{q}}g)$ . Introducing the set of Lagrange multipliers  $f_{\mathbf{q}}g$  each of which enforcing the value of  $h_{\mathbf{q}} = \langle h_{\mathbf{q}} \rangle$ , we write the partition function of the surface as

$$Z_G[\mathbf{A}_p; f_{\mathbf{q}}g] = \int \mathcal{D}[\mathbf{f}_{\mathbf{q}}g] \exp \left\{ -\frac{1}{4} H(\mathbf{f}_{\mathbf{q}}g) - \sum_{\mathbf{q}} h_{\mathbf{q}} j_{\mathbf{q}}^2 \right\}; \quad (19)$$

where  $\beta = (k_B T)^{-1}$ . The associated Gibbs free energy is

$$G[\mathbf{A}_p; f_{\mathbf{q}}g] = -k_B T \ln Z_G; \quad (20)$$

From Eqs.(19) and (20) it is easy to derive the following relation

$$h_{\mathbf{q}} = \langle h_{\mathbf{q}} \rangle = -\frac{dG}{dj_{\mathbf{q}}^2}; \quad (21)$$

and

$$\langle h_{\mathbf{q}} \rangle \langle h_{-\mathbf{q}} \rangle = \langle h_{\mathbf{q}} h_{-\mathbf{q}} \rangle = -k_B T \frac{d^2 G}{dj_{\mathbf{q}}^2 dj_{-\mathbf{q}}^2}; \quad (22)$$

The Helmholtz free energy  $F$  is related to  $G$  via

$$F[\mathbf{A}_p; h_{\mathbf{q}}] = G[\mathbf{A}_p; f_{\mathbf{q}}g] + \sum_{\mathbf{q}} h_{\mathbf{q}} j_{\mathbf{q}}^2; \quad (23)$$

where

$$\frac{dF}{dh_{\mathbf{q}}} = j_{\mathbf{q}}^2; \quad (24)$$

If we use expression (17) for the Helmholtz free energy, we find from Eq.(24) that

$$j_{\mathbf{q}}^2 = l^2 [q^2 + q^4 + O(q^6)] h_{\mathbf{q}} + \quad (25)$$

[note that  $h_{\mathbf{q}}(j_{\mathbf{q}} = 0) = 0$ ]. Combining Eqs.(17), (23), and (25) we obtain the following expression for Gibbs free energy

$$G = F[h_{\mathbf{q}}] - f_0 g + \sum_{\mathbf{q}} \frac{j_{\mathbf{q}}^2 j_{-\mathbf{q}}^2}{2l^2 [q^2 + q^4 + O(q^6)]} + O(j_{\mathbf{q}}^4); \quad (26)$$

When this expression for  $G$  is substituted in Eq.(22) and evaluated for  $f_{\mathbf{q}}g = f_0 g$  (which corresponds to the reference state  $h_{\mathbf{q}}g = f_0 g$ ), we find that the mean square amplitude of the fluctuations with a wave-vector  $\mathbf{q}$  (the "spectral intensity") is given by

$$\langle h_{\mathbf{q}} \rangle \langle h_{-\mathbf{q}} \rangle_{f_{\mathbf{q}}g=f_0g} = \langle h_{\mathbf{q}}^2 \rangle_{f_{\mathbf{q}}g=f_0g} = \frac{k_B T}{l^2 [q^2 + q^4 + O(q^6)]}; \quad (27)$$

This result, which quantifies the magnitude of the fluctuations around the flat equilibrium state, provides a second ("fluctuation") route for calculating  $\kappa$  and  $\gamma$  (but not for the saddle-splay modulus  $\bar{\kappa}$ ). It is frequently quoted in an incorrect form with  $\kappa_0$  and  $\gamma_0$ , the coefficients in the Helfrich Hamiltonian (1), instead of  $\kappa$  and  $\gamma$ . The equivalence of the two routes to membrane elasticity is expressed by the fact that the elastic coefficients appearing in expression (27) are the same as those obtained from Eqs.(9)-(11), and which are associated the "equilibrium" route. In the next section we use Eqs.(9)-(11) to derive statistical mechanical expressions for the elastic coefficients. Then, in section IV, we demonstrate, using computer simulations of a bilayer membrane model, the agreement between the two different methods of calculation.

### III. THERMODYNAMIC EXPRESSIONS FOR THE ELASTIC COEFFICIENTS

#### A. The surface tension

Let us return to the equilibrium route to membrane elasticity and to expressions (9)–(11) which describe the relation between the free energy and the elastic coefficients. The surface tension can be computed by comparing the free energy of the membrane at the reference state (which is assumed to be flat) and the free energy of a flat membrane with a slightly larger area. These two membranes are shown schematically, without the underlying microscopic details, in Figs. 1 (a) and (b). We reemphasize that the total number of amphiphilic molecules which form the membrane is fixed, and that the surface tension should be related to the free energy dependence on the area density of the amphiphiles (rather than the free energy cost to add molecules to the membrane). The characteristic surface of the membrane to which the free energy is applied, is chosen as the mid surface between the two layers. The total volume of the membrane is assumed to be fixed; otherwise, an additional term involving the volume compression modulus must be introduced in Eq.(6).

It is important to remember that in Figs. 1 (a) and (b), only the mean configurations of the surface (in the reference and deformed states) are depicted, and that the surface undulates around these (ensemble) average conformations. In other words, "the state of the surface" refers to its average conformation. As has been discussed earlier in section II, normal forces must be applied in order to deform the surface from its reference state [52]. If the membrane is embedded in a solution and placed in a container, then these forces can be generated by deforming the entire container, as demonstrated in Fig. 1 (d). Such a system can be conceptually divided into bulk aqueous phases and the interface between them which includes the membrane and the adjacent hydration layers. The volumes of the bulk phases above and below the membrane are fixed by the presence of solute particles that cannot permeate the membrane. The deformation of the boundaries of the container "percolates" to the interface and the latter acquires the shape of the surface of the container. However, since the bulk solution is fluid and has a vanishing shear modulus, its deformation without changing its volume does not add any contribution to the free energy.

Even though real bilayer systems are always embedded in a solvent (which influences their elastic properties), the calculation of the surface tension can be also performed for model systems that exclude the latter and leave only the interfacial region. This is possible due to the fact that the surface tension can be calculated by considering a deformed flat membrane. Such a membrane can be uniquely defined by the perimeter  $P = P(\mathbf{r})$  of the characteristic surface [represented by open circles in Fig. 1 (d)]. The free energy of the membrane can be derived from the partition function  $Z$  via the relation

$$F = -k_B T \ln Z; \quad (28)$$

The expression for the partition function must take into account the microscopic nature of the membrane, and the potential energy  $E$  due to the interactions between the amphiphilic molecules. In what follows we assume that  $E$  can be written as the sum of pair interactions between the atoms ("interaction sites") forming the molecules

$$E = \sum_{h < i}^X r_{hi}; \quad (29)$$

where  $r_{hi}$  is the distance between atoms  $h$  and  $i$ , and summation over all pairs of atoms  $h < i$  is performed. The various interactions are not identical but rather pair-dependent, as each amphiphilic molecule is typically composed of many different atoms. They also depend on whether the atoms belong to different molecules or part of the same amphiphile. In the latter case some atoms are covalently bonded what brings in an additional contribution to  $E$ . For brevity we will omit the subscripts of the potential and the indices of the argument  $r_{hi}$  will serve as an indicator of the specific potential. With the potential energy described by Eq.(29), the partition function is given by

$$Z = \sum_{P \text{ Conf:}}^X \exp \left[ -\sum_{h < i}^X r_{hi} \right] = k_B T A; \quad (30)$$

where the sum runs over all the conformations in which the perimeter of the characteristic surface is depicted by the closed curve  $P$ . Our assumption that the membrane has no spontaneous curvature guarantees that its average conformation is indeed flat. Alternatively, one may consider the system together with the bulk phases, and replace the sum in Eq.(30) with integration of the coordinates of all atoms  $\mathbf{r}$  over the entire volume of container (or the simulation cell)  $V_{\text{cell}}$

$$Z = \int_{V_{\text{cell}} = 1}^X d\mathbf{r} \exp \left[ -\sum_{h < i}^X r_{hi} \right] = k_B T A; \quad (31)$$

In addition to the above integral, it is necessary to specify the boundary conditions for the positions of the amphiphiles near the walls of the container, so that the perimeter of the characteristic surface would be described by  $P$ .

Let us assume that our cell (container) has a square cross section of linear size  $L_p$  with  $L_p = 2x; y < + L_p = 2$ . The deformation of the cell depicted in Fig. 1 (d) can be described by the following linear transformation

$$\begin{pmatrix} r_x \\ r_y \\ r_z \end{pmatrix} A = \begin{pmatrix} 0 & 1 & 0 \\ 1 & 0 & 0 \\ 0 & 0 & 1 \end{pmatrix} \begin{pmatrix} R_x \\ R_y \\ R_z \end{pmatrix} A; \quad (32)$$

which maps every point  $R$  on the boundaries of the undeformed cell to its strained spatial position  $r$ . The characteristic surface has the same shape as the upper and lower faces of the cell, and its area is given by

$$A = A_p \sqrt{1 + \frac{2}{L_p^2}} = A_p \left( 1 + \frac{2}{L_p^2} + O\left(\frac{4}{L_p^4}\right) \right); \quad (33)$$

where  $A_p = L_p^2$  is the area of the reference surface. Since the deformed surface which we consider is flat, its free energy is given by [see Eqs.(6) and (33)]

$$F = F(\epsilon = 0) + A_p \frac{\epsilon^2}{2}; \quad (34)$$

from which we conclude that

$$= \frac{1}{A_p} \frac{d^2 F}{d\epsilon^2} \Big|_{\epsilon=0}; \quad (35)$$

Using the relation between the free energy and the partition function (28), we may also write the above result in the following form

$$= \frac{k_B T}{A_p} \frac{1}{Z} \frac{d^2 Z}{d\epsilon^2} \Big|_{\epsilon=0} = \frac{1}{Z^2} \frac{dZ}{d\epsilon} \Big|_{\epsilon=0}^2; \quad (36)$$

If we now turn to our expression (31) for the partition function, we notice that it depends on  $\epsilon$  only through the integration volume  $V_{cell}$ . The differentiation of  $Z$  with respect to  $\epsilon$ , however, could be carried out more easily if the dependence on  $\epsilon$  is removed from  $V_{cell}$  and brought into the integrand. In other words, we wish to change the integration variables in (31) from  $r$  to  $R$ , where the latter are confined inside the undeformed cell. This is achieved using transformation (32), which originally described the deformation of the boundary points, and is now being applied inside the volume of integration [53]. With the new set of variables, the distance between two atoms is given by

$$r^2 = R^2 + 2 R_x R_z + \frac{2}{L_p^2} R_x^2; \quad (37)$$

In the undeformed reference state  $r(\epsilon = 0) = R$ . The partition function reads

$$Z = \frac{1}{V_0} \int_{V_0} d\mathbf{r} \exp\left[-\frac{U(\mathbf{r})}{k_B T}\right] = \frac{1}{V_0} \int_{V_0} d\mathbf{R} \exp\left[-\frac{U(\mathbf{R})}{k_B T}\right] \sqrt{\det J} \quad (38)$$

where  $V_0 = V_{cell}(\epsilon = 0)$  is the volume of the undeformed cell. The Jacobian of the transformation has been eliminated from the integrand in the above expression since it is unity. The differentiation of  $Z$  with respect to  $\epsilon$  is now straightforward but lengthy. We skip the details of the calculation, and write below the final expressions for the first and second derivatives, evaluated for  $\epsilon = 0$  [only the value at  $\epsilon = 0$  is required in Eq.(36)]

$$\frac{dZ}{d\epsilon} \Big|_{\epsilon=0} = \frac{1}{V_0} \int_{V_0} d\mathbf{R} \exp\left[-\frac{U(\mathbf{R})}{k_B T}\right] \frac{1}{k_B T} \frac{dU(\mathbf{R})}{d\epsilon} \Big|_{\epsilon=0}; \quad (39)$$



and

$$\begin{aligned} \frac{d^2 Z}{d^2} &= \frac{Z}{V_0} \frac{dV_0}{dR} \exp \left( \frac{4}{R} \right) \frac{X}{h_i} \frac{R^3}{5} \frac{R^2}{k_B T} \frac{R_x R_z}{R} \frac{R^2}{5} \\ &= \frac{1}{A_p k_B T} \frac{X}{h_i} \frac{R^3}{5} \frac{R_x R_z}{R} \frac{R^2}{5} + \frac{1}{A_p k_B T} \frac{X}{h_i} \frac{R^3}{5} \frac{R_x^2}{R} \frac{R^2}{5} + \frac{1}{A_p k_B T} \frac{X}{h_i} \frac{R^3}{5} \frac{R_z^2}{R} \frac{R^2}{5} ; \end{aligned} \quad (40)$$

where  $\frac{dV_0}{dR} = \frac{dV_0}{dR}$  and  $\frac{d^2 V_0}{dR^2} = \frac{d^2 V_0}{dR^2}$ . When these expressions are substituted into Eq.(36) we readily find that

$$\begin{aligned} &= \frac{1}{A_p k_B T} \frac{X}{h_i} \frac{R^3}{5} \frac{R_x R_z}{R} \frac{R^2}{5} + \frac{1}{A_p k_B T} \frac{X}{h_i} \frac{R^3}{5} \frac{R_x^2}{R} \frac{R^2}{5} + \frac{1}{A_p k_B T} \frac{X}{h_i} \frac{R^3}{5} \frac{R_z^2}{R} \frac{R^2}{5} \\ &+ \frac{1}{A_p k_B T} \frac{X}{h_i} \frac{R^3}{5} \frac{R_x R_z}{R} \frac{R^2}{5} + \frac{1}{A_p k_B T} \frac{X}{h_i} \frac{R^3}{5} \frac{R_x^2}{R} \frac{R^2}{5} + \frac{1}{A_p k_B T} \frac{X}{h_i} \frac{R^3}{5} \frac{R_z^2}{R} \frac{R^2}{5} ; \end{aligned} \quad (41)$$

where the thermal averages are evaluated at the undeformed reference state of the system ( $\epsilon = 0$ ). If the system is macroscopically invariant with respect to reversal of the sign of the  $z$  coordinates ( $z \rightarrow -z$ ), then the first term in the above expression for  $\gamma$  vanishes. If, in addition, the system is invariant with respect to rotation around the  $z$  axis ( $x \rightarrow y; y \rightarrow -x$ ), then another expression can be derived with  $R_x$  replaced by  $R_y$ . Defining  $R_t = \sqrt{R_x^2 + R_y^2}$ , we finally arrive to the following expression:

$$\begin{aligned} &= \frac{1}{2A_p k_B T} \frac{X}{h_i} \frac{R^3}{5} \frac{R_x R_z}{R} \frac{R^2}{5} + \frac{1}{2A_p k_B T} \frac{X}{h_i} \frac{R^3}{5} \frac{R_y R_z}{R} \frac{R^2}{5} \\ &+ \frac{1}{2A_p k_B T} \frac{X}{h_i} \frac{R^3}{5} \frac{R_t R_z}{R} \frac{R^2}{5} + \frac{1}{2A_p k_B T} \frac{X}{h_i} \frac{R^3}{5} \frac{R_t^2}{R} \frac{R^2}{5} \\ &+ \frac{1}{2A_p k_B T} \frac{X}{h_i} \frac{R^3}{5} \frac{R_t R_z}{R} \frac{R^2}{5} : \end{aligned} \quad (42)$$

This expression can be also written in the following compact form

$$\gamma = L_z \frac{C_{xxzz} + C_{yyzz}}{2} \frac{P_{xx} - P_{yy}}{2} L_z \gamma_{zt}; \quad (43)$$

where  $L_z$  is the linear size of the system (the cell) in the  $z$  direction (normal to the membrane), while  $P$  and  $C$  denote the pressure tensor and the tensor of elastic constants of the system. The quantity  $\gamma_{zt}$  is the shear modulus associated with the deformation depicted at Fig. 1 (d) [42, 49].

It is interesting to compare the above results (42)-(43) with the much better known (and more frequently used) expression for the surface tension [28, 34]

$$\gamma = \frac{1}{2A_p} \frac{X}{h_i} \frac{R^3}{5} \frac{R_t^2}{R} \frac{R^2}{5} = L_z \frac{2P_{zz} - P_{xx} - P_{yy}}{2} L_z \gamma_{zt}; \quad (44)$$

The latter expression is obtained when one considers the variation of the free energy resulting from the (volume-preserving) variation of the projected area  $A_p$

$$\gamma \sim \frac{\partial F}{\partial A_p} \quad ; \quad (45)$$

The deformed state associated with the surface tension  $\gamma$  is shown in Fig. 1 (c). For fluid membranes we anticipate that  $\gamma = \gamma_{xz}$  since the difference between them

$$\gamma_{xz} = L_z \frac{C_{xxxx} + C_{yyyy}}{2} = P_{zz} - L_z \gamma_{yz} ; \quad (46)$$

is proportional to the shear modulus  $\gamma_{yz}$  associated with the deformation shown in Fig. 1 (e). The shear modulus  $\gamma_{yz}$  is expected to vanish because the areas of the characteristic surfaces of the membranes in Figs. 1 (a) and (e) are identical; and the Helfrich free energy of a flat membrane depends only on the area of the characteristic surface, but not on the orientation of the plane of the membrane with respect to the walls of the container. This argument for the coincidence of  $\gamma$  and  $\gamma_{xz}$  could be applied directly to the membranes in Figs. 1 (b) and (c), whose characteristic areas (as well as their volumes) are also identical. The tilt of the cell's wall, however, can be safely ignored only in the thermodynamic limit, when the width of the membrane becomes much smaller than its lateral dimensions. If the system is not sufficiently large than the Helfrich form for the free energy in which the membrane is associated with a 2D characteristic surface is not entirely applicable. The finite width of the membrane must show up in the expression for the free energy, and the surface tensions  $\gamma$  and  $\gamma_{xz}$  do not perfectly agree.

#### B . The bending modulus

The bending modulus can be calculated by considering a deformation of the characteristic surface from a flat to cylindrical geometry. The deformation, which is depicted in Fig. 2, can be described by the following nonlinear transformation of the boundaries of the cell [compare with Eq.(32)]

$$\begin{aligned} r_x &= R_x \\ r_y &= R_y \\ r_z &= R_z + \frac{L_p^2}{R_0^2} x^2 = \frac{L_p^2}{R_0^2} x^2 + R_0^2 ; \end{aligned} \quad (47)$$

where  $L_p = 2 \sqrt{R_0^2 - R_z^2}$ , and  $R_0 = L_p$  is the radius of curvature of the cylinder. The integrated total curvature [Eq.(7)] of the characteristic surface is

$$J = \frac{L_p}{R_0} ; \quad (48)$$

and its area is

$$A = A_p + 2 \arcsin \frac{L_p}{2R_0} = A_p \left( 1 + \frac{1}{24} J^2 + O(J^4) \right) ; \quad (49)$$

The free energy is, hence, given by

$$F = \frac{L^2}{24} + \frac{1}{2} J^2 + \dots ; \quad (50)$$

from which we deduce the following relation

$$\frac{L^2}{12} + \dots = \frac{1}{A_p} \frac{d^2 F}{dJ^2} \Big|_{J=0} ; \quad (51)$$

where

$$J = \frac{1}{R_0} ; \quad (52)$$



depend neither on the shape of the membrane nor on the location of the origin is obtained as follows: The first and third terms in Eq.(59) can be written jointly in the following form

$$\frac{X_i X_j}{h_i h_j} \frac{1}{R_i} \frac{1}{R_j} \frac{R_x R_z R_x R_z}{R R} \frac{L^2}{12} X_i X_j = \quad (60)$$

$$\frac{X_i X_j}{h_i h_j} \frac{1}{R_i} \frac{1}{R_j} \frac{R_x R_z R_x R_z}{R R} \frac{L^2}{12} X_i^2 + X_j^2; \quad (61)$$

where

$$X_i^2 = \frac{X_i^2 + X_j^2}{2}; \quad (62)$$

and

$$X_j^2 = \frac{X_i^2 + X_j^2}{2}; \quad (63)$$

The terms appearing before the square brackets in Eq.(61) depend only on the relative coordinates of atoms with respect to each other. Therefore, the average of  $X_i^2$  (the second term in square brackets, which depends only the location of the center of the pair/triplet/quartet in question) can be performed separately. As in Eq.(57) we have  $X_i^2 = L_p^2 = 12$ , what leads to the cancellation of the first two terms in square brackets in Eq.(61). Applying the same argument for the second and fourth terms in Eq.(59), and defining  $Y_i^2 = Y_i^2 + Y_j^2 = 2$ , and  $Y_j^2 = Y_i^2 + Y_j^2 = 2$ , we arrive to the following expression

$$= \frac{1}{2A_p k_B T} \frac{X_i X_j}{h_i h_j} \frac{1}{R_i} \frac{1}{R_j} \frac{R_z R_z}{R R} R_x R_x X_i^2 + R_y R_y Y_j^2; \quad (64)$$

which is the more general form for expression (59) since it is independent of the shape of the membrane and of the location of the origin of axes.

The deformed membrane, shown schematically in gray shade in Fig. 2, may be considered as part of a closed cylindrical vesicle (depicted by the dashed line Fig. 2). Accordingly, one may argue that its free energy is given by

$$F = \frac{\alpha}{2} F_{\text{vesicle}} \quad (65)$$

where  $F_{\text{vesicle}}$  is the free energy of the vesicle and  $\alpha$  is the apex angle of the deformed membrane. This relation, however, is incorrect since  $F_{\text{vesicle}}$  includes a term which is unique to closed vesicles and should be omitted in the case of open membranes. The additional contribution to  $F_{\text{vesicle}}$  which has been termed "the area-difference elastic energy", should not be confused with the bending energy. The latter is the free energy required to bend the membrane while keeping its area density fixed. The former, on the other hand, originates from the simple fact that upon closure of the vesicle, it becomes impossible to preserve the area densities of the amphiphiles in both the outer and the inner monolayers. The outer monolayer is stretched and the inner monolayer is compressed relative to the mid characteristic surface. The elastic energy resulting from such curvature-induced changes in the monolayer areas is a non-local effect because the monolayers are capable of independent lateral redistribution to equalize the area per molecule of each leaflet. The distinction between (local) bending elasticity and (non-local) area-difference elasticity has been discussed by Helfrich, not long after introducing his famous Hamiltonian [54]. The idea, however, did not gain much popularity until the issue has been analyzed systematically by Svetina et al. some years later [55]. Early theoretical works and experimental measurements of the bending modulus failed to separate the local and non-local contributions [56]. This is not the case with our expression (64) for which has been derived by considering an open membrane. For an open membrane, the two leaflets have the same area as the top (bottom) surface of the containers and, consequently, area-difference elasticity do not show up.

### C . The saddle-splay modulus

Finally, we derive our expression for the saddle-splay modulus . The following transformation, applied to the boundaries of the container

$$\begin{aligned} r_x &= R_x \\ r_y &= R_y \\ r_z &= R_z + \frac{q}{R_0^2} \frac{x^2}{2} + \frac{q}{R_0^2} \frac{y^2}{2} \end{aligned} \quad (66)$$

(with  $L_p=2$   $x < +L_p=2$ ), describes a deformation of the surface to spherical geometry where the sphere's radius  $R_0 = L_p$ . It is not difficult to show that the free energy of the spherical surface is given by

$$F = A_p \left( \frac{L^2}{12} + 2 + H^2 \right); \quad (67)$$

where  $H = 1/R_0$ . From the above expression for  $F$ , the following relation

$$\frac{L^2}{6} + 4 + 2 = \frac{1}{A_p} \frac{d^2 F}{dH^2} \Big|_{H=0}; \quad (68)$$

is easily derived. The deformed pair distance is

$$r = R^2 - 2X(R_x + Y(R_y - R_z)H + X(R_x + Y(R_y - R_z)H^2)^{1/2}; \quad (69)$$

where  $X$  and  $Y$  have been defined in section IIIB. Since Eqs.(68) and (69) have, respectively, the same form as Eqs.(51) and (53), we immediately conclude that the r.h.s of Eq.(68) is given by expression similar to (55) in which  $X - R_x$  is everywhere exchanged with  $X - R_x + Y(R_y - R_z)$ . Following the same steps described in the derivation of Eq.(59) from (55), and using the additional relation

$$X - Y = \frac{1}{L_p^2} \int_{L_p=2}^Z \int_{L_p=2}^Z xy dx dy = 0; \quad (70)$$

we finally arrive to the following result

$$= \frac{1}{A_p k_B T} \left( \frac{X}{R} \right)^2 \Big|_{h_i}^0 - \frac{X}{R} \left( \frac{R_x}{R} \right)^2 \Big|_{h_i}^0 - \frac{Y}{R} \left( \frac{R_y}{R} \right)^2 \Big|_{h_i}^0; \quad (71)$$

This expression applies to square membranes only, with the origin located at the center of the membrane. The more general expression is

$$= \frac{1}{A_p k_B T} \left( \frac{X}{R} \right)^2 \Big|_{h_i}^0 - \frac{R_z}{R} \left( \frac{R_z}{R} \right)^2 \Big|_{h_i}^0 - \frac{R_x}{R} \left( \frac{R_x}{R} \right)^2 \Big|_{h_i}^0 - \frac{R_y}{R} \left( \frac{R_y}{R} \right)^2 \Big|_{h_i}^0; \quad (72)$$

### IV . NUMERICAL RESULTS

The purpose of the MC simulations which we conducted and present in this section is twofold: The first is to test the validity and accuracy of our expressions for the elastic coefficients. The second is to examine the agreement between the mechanical and the fluctuation routes to membrane elasticity, as discussed in section II. The model system whose elastic properties were studied by the simulations has been described in great details in Ref. [47]. Briefly, the "lipids" that serve as the building blocks of the membrane consist of three spherical atoms of diameter  $a$  (see Fig. 3) interacting with each other via pair-wise LJ potentials (whose details can be found in Ref. [47]). To avoid the complications involved with long-range interactions, the LJ potentials have been truncated at some cut-off separation  $R = r_c = 2.5a$  and, in addition, modified to ensure the vanishing of  $\phi$  and its first two derivatives,  $\phi'$  and  $\phi''$ , at  $r_c$ . The continuity of the second derivative of the pair potentials is an important feature since  $\phi''$

appears in our expressions (42) for  $\gamma$ . Two changes have been made in comparison to the original model presented in Ref. [47]. The first is a small reduction of the temperature which, in this paper, has been set to  $0.9T_0$  where  $T_0$  is the original temperature (in Ref. [47]). The second is the addition of new interactions between atoms which are part of the same molecule. In Ref. [47] the molecules were linear rigid trimers with a fixed distance  $a$  between the centers of the constituent atoms. Here, we allow some little variations of the separation between the atoms. The mid atom (labeled 2) has been linked to the two end atoms (labeled 1 and 3) via harmonic springs with spring constant  $K$  and equilibrium length  $a$ :

$$V(R) = \frac{1}{2}K(R - a)^2; \quad (73)$$

while the pair potential between the end atoms has been set to

$$V(R) = \frac{1}{2}K(R - 2a)^2; \quad (74)$$

We use a large value for the spring constant  $K = 8000 k_B T/a^2$ , for which the separations between the atoms do not exceed the order of 1% of their equilibrium values. While this means that the molecules in our model are "almost" linear and rigid, the use of the above potentials (73) and (74) creates a situation in which all inter-atomic interactions (whether between atoms belonging to the same or different molecules) are depicted by smooth potentials; and so, our expressions for the elastic constants can be used without any further complications. The total number of lipids in our simulations was  $N = 1000$  (500 lipids in each monolayer), and no additional solvent molecules were included inside the simulation cell (as if the membrane is vacuum). Periodic boundary conditions were applied in the plane of the membrane, and no boundaries for the simulation cell were defined in the normal direction. The linear size of the (square) membrane was set to  $L_p = 29.375a$ . Subsequent MC configurations were generated by two types of moves: translations of lipids (which also included some minute changes in the relative locations of the three atoms with respect to each other) and rotations around the mid atom. A set of  $2N = 2000$  move attempts of randomly chosen molecules is defined as the MC time unit. Both types of moves (translations and rotations) were attempted with equal probability, and the acceptance probabilities of both of them was approximately half. The MC relaxation time has been evaluated in Ref. [47]. It is of the order of  $10^4$  MC time units and has been very little affected by the changes introduced in the model. A typical equilibrium configuration of the membrane is shown in Fig. 4.

#### A. The fluctuation route

The fluctuation approach for determining the surface tension and the bending modulus is straightforward to implement: The profile of the membrane in our simulations was defined by mapping the system onto an  $8 \times 8$  grid, and defining the height  $h(\mathbf{r}_g)$  of the membrane in each grid cell as the average of the local heights of the two monolayers. The latter were evaluated by the mean height of the lipids (whose positions were identified with the coordinates of their mid atoms) belonging to each layer, which were instantaneously located inside the local grid cell. Note that the mesh size  $l = L_p/8 = 3.67a$  is somewhat larger than the size of the lipids, as required in our discussion in section II. The Fourier transform of  $h(\mathbf{r}_g)$  was obtained using Eq.(18), and the mean squared amplitudes of the different modes were, eventually, fitted to the inverse form of Eq.(27)

$$\frac{1}{l^2 \langle h_q^2 \rangle} = \frac{l^2 [q^2 + q^4 + O(q^6)]}{k_B T}; \quad (75)$$

The results of this spectral analysis are summarized in Fig. 5, where we plot the value of  $l^2 \langle h_q^2 \rangle$  as a function of  $q^2$ . The error bars represent one standard deviation in the estimates of the averages, which were obtained from simulations of 16 different membranes and a total number of  $1.25 \times 10^4$  measurements of the spectrum per membrane. The measurements were done at time intervals of 100 MC time units. The curve depicts the best fit to Eq.(75), which is obtained when  $\gamma$  and  $\kappa$  take the following values:

$$\begin{aligned} \gamma &= (0.6 \pm 0.2) \frac{k_B T}{a^2} \\ \kappa &= (46 \pm 2) k_B T; \end{aligned} \quad (76)$$

The contribution of the  $q^6$  term to the fit was, indeed, significantly smaller than that of the other two terms on the r.h.s. of Eq.(75).

## B . The equilibrium route

While the measurement of  $\gamma$  and  $\kappa$  using the fluctuation approach was a relatively straightforward matter, the application of the equilibrium approach emerged as somewhat more challenging task. The most significant differences between the two approaches was the amount of computer resources required for an accurate determination of the elastic coefficients. The results which we present in this section have been obtained using 64 nodes on a Beowulf cluster consisting of Intel architecture PCs, where the CPU time per node was of the order of three months. The need of such a large computer time should be compared to the relative ease with which the results in Eq.(76) have been obtained – using a total number of only 16 nodes over a period of about 10 days. The reason that the equilibrium approach is so much computer-time-consuming is the "noisy" nature of the statistics of the terms whose averages are evaluated in expressions (42) and (59). From the conceptual point of view, the determination of the surface tension using expression (42) is pretty simple. The determination of the surface tension  $\gamma$  from expression (44) is even easier since it is a much less noisy quantity. In fact, the computational effort required for an accurate determination of the value of  $\gamma$  is even smaller than the one required for the calculation of  $\kappa$  by the fluctuation method. The surface tension  $\gamma$  does not apply directly to membranes with a fixed projected area. Yet, it is expected to coincide with  $\gamma_{\text{th}}$  in the thermodynamic limit.

The determination of  $\kappa$  is more complicated. Here we can, in principle, choose between expressions (59) and (64). The latter is more general (since it is not restricted to square membranes), but prohibitively time consuming. This can be understood by considering the number of operations required for a single measurement of the quantities of interest. Assuming each atom in our simulations interact with a finite number of other atoms, the total number of operations required by expression (64) is  $O(N^2)$ , while the number required by expression (59) is only  $O(N)$ . In our simulations the total number of atoms is 3000, which means a difference of about 4 orders of magnitude in efficiency. Using expression (59) to measure  $\kappa$  is, however, tricky because this expression involves not only the relative locations of the particles with respect to each other (as in the case of the expressions for the surface tension), but also the absolute coordinates of atoms. This would not create a problem if only the central coordinates ( $X$  and  $Y$ ) of the pairs had to be found [as one may, naively, conclude from Eq.(59)], since that among the set including the pair  $(i; j)$  and all its periodic images, only one satisfies the requirement  $L_p/2 \leq X_j - X_i \leq L_p/2$ . However [and this becomes clear from the derivation of expression (64) from expression (59)], what we actually have here is a periodic boundary conditions problem where the pairs play the role of the particles, and  $X$  and  $Y$  serve as the coordinates of these "particles". This means that each quartet  $((i; j); (i'; j'))$  is identified as the pair  $(i; j)$  and the pair  $(i'; j')$  or its image nearest to  $(i; j)$  and, in addition, that the center of the quartet must satisfy  $L_p/2 \leq X_{j'} - X_i \leq L_p/2$ . The fact that sometimes a pair must be replaced by one of its images (which are located outside the boundaries of the simulation cell) is problematic since this means that the location of the pair, which is needed in expression (59), cannot be specified by a single value. A solution to this problem is obtained by dividing the simulation cell into stripes parallel to either the  $x$  or the  $y$  axes [depending on whether we calculate the third or fourth term in Eq.(59)], and to split the summation over all the pairs to several partial sums over the pairs included in the different stripes. The partial sum corresponding to the images of each stripe (which consist of all the images of the pairs included in the stripe) can be found with almost no additional effort. The product of two partial sums gives the contribution of all the quartets consisting of pairs located inside the two relevant stripes. Depending on the distance between the stripes (along the relevant axis) and their locations with respect to the center of the cell, it is usually easy to decide in which case a stripe should be replaced by one of its images. Ambiguities about the correct decision occur in a finite number of cases (i.e., for a finite number of pairs of stripes). In these cases, individual decisions must be made for each quartet. The number of such quartets can be reduced significantly if the system is divided into a large number of stripes  $N_s$ , since the narrower the stripes the smaller the number of pairs included in each one of them. A more elegant solution is to choose a certain convention about the ways the contribution from the ambiguous quartets is added to Eq.(59). This will inevitably introduce a systematic error to our estimates of  $\kappa$ . However, if we make a set of estimates based on increasingly larger values of  $N_s$ , we can obtain the correct averages by extrapolating our results to the limit  $1/N_s \rightarrow 0$ . The method, which is described in more details in the Appendix, can be generalized to handle correctly the calculation of  $\kappa$ . However, because of the mixing of the  $x$  and  $y$  coordinates in Eq.(71), the implementation of the method becomes more complicated. For this reason, and due to the fact that the fluctuation approach does not provide a value of saddle-splay modulus to compare with, we did not use our simulations to calculate  $\kappa$ .

In section II we have explained in great details why the elastic coefficients obtained from the fluctuation approach are the free energy coefficients  $\kappa_f$  and  $\gamma_f$  rather than the Hamiltonian coefficients  $\kappa_0$  and  $\gamma_0$ . This means that the quantities in expressions (42) and (59) should be averaged over the ensemble of all possible microscopic configurations. However, it is also easy to understand that the same expressions can be used to calculate the Hamiltonian coefficients. The latter, which characterize the energy changes caused by deformations of the flat membrane, can be obtained by restricting the averages to conformations where  $h(\mathbf{r}_g) = 0$  for every grid cell, thus avoiding the entropic contribution of the thermal fluctuation to the free energy. To sample this conformation phase space one need to accompany every

MC move attempt with one or two (depending on whether the molecule leaves the grid cell or not) additional moves of adjacent molecules. Moreover, one can also sample the phase-space consisting of only those conformations of the membrane with wave vectors in the range  $2\pi L_p < q$ . The results of such a calculation are the wave-dependent coefficients  $\gamma(q)$  and  $\tilde{\gamma}(q)$ . One of the problems which can be studied by such investigation is the value of the numerical coefficient  $c$  in the formula for the renormalized bending modulus [57, 58, 59, 60]:

$$\gamma(q) = \gamma_0 + c \frac{k_B T}{4} \ln(q L_p) \quad (77)$$

This problem aroused a renewed interest recently since it has been suggested that the value of  $c$  may be positive, which means (quite remarkably) that the fluctuations stiffen rather than soften the membrane [61, 62, 63].

While determining the value of  $c$  was not possible with our computer resources, we did use Eq.(77) in our analysis of the results. Our need of Eq.(77) and the link that it provides between  $\gamma_0$  and  $\gamma(q)$  is related to the peculiar nature of our simulations which are made in a "solvent-free" environment. As has been discussed in section III, our expressions for the elastic coefficients have been derived based on the assumption that the membrane is embedded in solvent and that the entire container is deformed. In our simulations, however, we have no container (there are no boundaries for the simulation cell in the  $z$  direction) and, so, the applicability of our approach should be examined carefully. The arguments which we presented in section IIIA [see, in particular, the discussion around Eq.(30)] demonstrate that the presence of solvent is essential only for the calculation of  $\gamma_0$  and  $\tilde{\gamma}_0$ , but not for the calculation of the surface tensions  $\gamma(q)$  and  $\tilde{\gamma}(q)$ . By contrast, the Hamiltonian coefficients can be all measured in a "solvent-free" model since they are extracted from simulations of flat, non-fluctuating, membranes. The value of  $\gamma_0$  and the relation given by Eq.(77) provide then an estimate for the value of  $\tilde{\gamma}_0$ . Since the finite-size correction to the value of  $\gamma_0$  grows only logarithmically with the size of the system, and since  $\gamma_0 \sim k_B T$ , the difference between  $\gamma_0$  and  $\tilde{\gamma}_0$  is not significantly large. In our simulations it actually falls within the uncertainty in our estimates of the bending modulus, which means that  $\gamma_0$  and  $\tilde{\gamma}_0$  are practically indistinguishable. In addition to our measurement of  $\gamma_0$ , we also measured  $\tilde{\gamma}_0$  directly from the simulations. As we have just explained above, such a measurement is expected to fail and to lead to the incorrect conclusion that  $\tilde{\gamma}_0 = 0$ . We used this incorrect result as a test for our code.

The values of the elastic coefficients have been extracted from simulations of 64 membranes starting at different initial configurations. The initial configurations were generated by randomly placing 500 lipids in two different layers with a vertical (along the  $z$  direction) separation  $a$  (the size of the atoms) between them. The initial configurations were "thermalized" over a period of  $2 \cdot 10^6$  MC time units, followed by a longer period of  $1.2 \cdot 10^6$  time units during which quantities of interest were evaluated. The uncertainties in our final results correspond to one standard deviation in the estimates of the averages. We first made the simulations with non-fluctuating membranes, from which we extracted the values of the Hamiltonian coefficients. Then, we removed the part in our algorithm which is responsible for keeping the membrane flat. The membranes were equilibrated again, and then the values of the thermodynamic (free energy) coefficients were determined.

For the bare coefficients we find the following values for the surface tension:

$$\begin{aligned} \gamma_0 &= (0.8 \pm 0.5) \frac{k_B T}{a^2} \\ \tilde{\gamma}_0 &= (-0.07 \pm 0.01) \frac{k_B T}{a^2} \end{aligned} \quad (78)$$

The comparison of these results with each other, and with the values of the elastic coefficients extracted from the fluctuation approach [Eq.(76)] reveals: (a) a disagreement between the two surface tensions  $\gamma_0$  and  $\tilde{\gamma}_0$ , which should be attributed to the finite size of our membrane (see our discussion in section IIIA); and (b) a disagreement between  $\gamma_0$  and  $\tilde{\gamma}_0$  which should be attributed to the entropic contribution to the surface tension. The bending modulus  $\kappa_0$  has been obtained by dividing the system into  $N_s$  stripes and extrapolating the results for  $\kappa_0$  to the limit  $1/N_s \rightarrow 0$ , as explained earlier in this section (see also the Appendix). From the extrapolation procedure, which is summarized in Fig. 6, we find that

$$\kappa_0 = (44 \pm 10) k_B T \quad (79)$$

This result also serves as our estimate for  $\tilde{\kappa}_0$  (see discussion earlier in this section). The similarity of the above value of  $\kappa_0$  (which is, unfortunately, obtained with a somewhat large numerical uncertainty) to the one quoted in Eq.(76) corroborates the argument presented in section II regarding the equivalence of the two routes to membrane elasticity. Further support to this argument is obtained from the agreement of our result in Eq.(76) to  $\tilde{\kappa}_0$ , with the value of the surface tension obtained from equilibrium approach [using expression (42)]:

$$\tilde{\kappa}_0 = (-0.3 \pm 0.5) \frac{k_B T}{a^2} \quad (80)$$



Our result for  $\gamma$  [expression (44)] is not very much different

$$\gamma = (0.41 \pm 0.01) \frac{k_B T}{a^2} : \quad (81)$$

These values are quite different from those given in Eq.(78), thus demonstrating the importance of the entropic contribution to the surface tension.

Finally, we plot in Fig. 7 our results for the "apparent" bending modulus  $\kappa$  which we have obtained, using expression (59), from simulations of a fluctuating membrane. These simulations serve as a test for our code. We find  $\kappa = (4 \pm 8) k_B T$  which is consistent with the anticipated value  $\kappa = 0$ .

## V. SUMMARY AND DISCUSSION

Motivated by the lack of a well accepted theory to deal with the statistical mechanical behavior of curved interfaces, we have studied the elastic properties of fluid bilayer membranes using analytical and computational tools. Two distinct methods have been employed to measure the surface tension  $\gamma$ , and the bending modulus  $\kappa$ , of a model membrane. In the "fluctuation" method the elastic coefficients were extracted from the analysis of the spectrum of thermal fluctuations of the membrane. The second ("equilibrium") method is based on the fact that  $\gamma$  and  $\kappa$  describe the free energy variations due to area-changing and curvature-forming deformations and, therefore, can be related to the derivatives of the partition function with respect to the relevant strain variables. Using this kind of relation, we have derived formal expressions for  $\gamma$  and  $\kappa$  in central force systems. Our expressions associate the elastic coefficients to the interactions between the molecules and the two-, three-, and four-particles distribution functions. The most important feature of these expressions is the fact that even though  $\gamma$  and  $\kappa$  (as well as the saddle-splay modulus  $\bar{\kappa}$ ) are related to deformations of the membrane, they can be extracted from a single MC run performed on the reference (unstrained) system.

One of the puzzles about curved interfaces elasticity is related to the correspondence between the above two approaches for determining their rigidity constants. We used linear response theory to prove that the two methods must agree for the values of  $\gamma$  and  $\kappa$  provided that the system is deformed by the application of external forces and not by altering other thermodynamic variables such as the temperature or the chemical potential of surface molecules. Moreover, our discussion clarifies that the coefficients in question,  $\gamma$  and  $\kappa$ , are the effective elastic coefficients which appear in the Helfrich free energy (rather than the Helfrich Hamiltonian) and which are influenced by the thermal undulations of the membrane. Our computer simulations and the numerical values of the elastic coefficients which we find, confirm the idea of equivalence between the two routes to membrane elasticity.

Comparison of the computational efficiency of the two methods shows that for our membrane model system the fluctuation method provides more accurate estimates of the elastic coefficients than the equilibrium method, and requires less CPU time. The major shortcomings of the fluctuation approach is the fact that it can be utilized for measurements of the effective coefficients only, and that it requires the determination of the profile of the interface during the course of the simulations. While this is easy with our "water-free" computer model, this may not be so in other cases, for instance, for membranes which tend to exchange molecules with the embedding solvent, or for liquid-vapor interfaces near the critical point when the interface is difficult to distinguish from the bulk phases. In these cases the equilibrium method may be more attractive since the interactions in the bulk phases do not contribute to the values of  $\gamma$  and  $\kappa$  when calculated using our expressions for the elastic coefficients. Moreover, with the same mechanical expressions for  $\gamma$  and  $\kappa$ , the bare (Hamiltonian) coefficients can be also calculate. Our measurements demonstrate that close to the tensionless state of the membrane, the entropic component of the surface tension is quite significant. This has been also found recently in a theoretical study of the surface tension of fluctuating surfaces [15].

Finally, we would like to reemphasize that our expressions for the elastic coefficients apply for central force systems only. Following our derivation one should be able to generalize them to more complicated cases including many-body interactions. A more realistic model must also include electrostatic interactions whose long-range nature pose a computational challenge.

Acknowledgments: We thank Ram Seshadri for his comments on the manuscript, and to Jeffrey Barteet for computational support in the Materials Research Laboratory (MRL). This work was supported by the National Science Foundation under Award No. DMR-0203755. The MRL at UC Santa Barbara is supported by NSF No. DMR-0080034.

# APPENDIX A : DETERMINATION OF $\gamma$ USING THE METHOD OF STRIPES

The most common way to reduce finite size effects in computer simulations is obtained by employing periodic boundary conditions, namely by regarding the simulation cell as part of an infinite periodic lattice of identical cells. When the range of the interactions is less than  $L_p=2$  (half the linear size of the cell) then each particle interacts only with the nearest periodic image of any other particle. This, in turn, is identified as the pair  $(i; j)$ . Each pair has infinitely many periodic images each of which is associated with a different simulation cell; and with each simulation cell each pair is associated exactly once. The set of all the different pairs associated with one of the cells [say, the original ("primitive") cell] is the one over which the summation in expressions (42) and (44) for the surface tension should be performed.

Things become more complicated when we try to evaluate the bending modulus using expression (59). In this case, coordinates associated with the location of the pair  $(X$  and  $Y)$  appear in the expression, and so it becomes necessary to decide which of the periodic images of each pair is actually associated with primitive simulation cell ( $-L_p/2 \leq X < +L_p/2$ ) over which the sum in Eq.(59) is performed. The intuitive candidate is the periodic image with  $-L_p/2 \leq X < +L_p/2$ . Making this choice, however, is not the right convention. The correct way to handle the summation in expression (59) can be deduced from our derivation of expression (64) which is independent of the location of the origin of axes. Following the discussion that led from Eq.(59) to Eq.(64) it becomes clear that: (a) each quartet  $((i; j); (i'; j'))$  must be reproduced exactly twice from sums in Eq.(59) [or once, if the quartets  $((i; j); (i'; j'))$  and  $((i; j); (i'; j'))$  are treated as different], and (b) that the central coordinate of the quartet,  $(X_c; Y_c)$ , must lie inside the region of the primitive simulation cell. These requirements can be perceived as if we have a periodic boundary condition problem with the pairs playing the role of particles and with  $(X; Y)$  serving as the coordinates of the pairs. What can also be learned from expression (64) is the fact that  $\gamma$  is associated with pair-pair correlations. Therefore, its accurate measurement is difficult in systems whose linear  $L_p < 2$ , where  $\gamma$  is the relevant correlation length. We proceed our discussion assuming that our system is sufficiently large and obeys the above criterion.

In order to calculate the third term in Eq.(59) we divide our system into an even number of stripes  $N_s = 2M$  ( $M$ -integer) parallel to the  $x$  axis, as shown in Fig. 8. The fourth term in Eq.(59) is calculated in the same manner by dividing the system into the same number of stripes parallel to the  $y$  axis. In addition to the primitive cell we also need to consider the nearest periodic extensions of linear size  $L_p=2$ . These periodic extensions, which are also shown in Fig. 8, consist of periodic images of the stripes. We label the stripes included in the primitive cell with the numbers  $M+1; \dots; 3M$ , the stripes on the right periodic extension with  $1; \dots; M$  (they are the periodic images of stripes  $2M+1; \dots; 3M$ ), and the stripes on the left periodic extension (the images of stripes  $M+1; \dots; 2M$ ) with  $3M+1; \dots; 4M$ . For each pair we calculate the quantity  $p = \frac{R_x - R_z}{R_x + R_z} = R$ . The location of the pair, which is identified with the mid-coordinate  $X = \frac{X_i + X_j}{2}$ , defines the stripe with which the pair should be associated. In Fig. 8 each pair is depicted as a particle. The pair labeled  $a$ , for instance, is located in the  $i$ th stripe, whereas its periodic image  $a^0$  is located in stripe number 13. For each stripe  $i$  in the primitive cell we calculate the sum

$$S_i = \sum_{\text{pairs in stripe } i} \frac{X}{L_p} \quad (A1)$$

The sum corresponding to stripe  $j$ , the image of stripe  $i$ , is given by

$$S_j = \sum_{\text{pairs in stripe } i} \frac{X}{L_p} \quad (A2)$$

where the sign  $(\pm)$  in the above expression depends on whether the image is situated to the right or the left of the primitive cell. The product  $p_{pq}$  gives the contribution to the third term in Eq.(59) of the quartets whose constituent pairs are included, respectively, in stripes  $p$  and  $q$ . These contributions should be in accord with requirements (a) and (b), mentioned in the previous paragraph, about the quartets and their locations. In some cases these requirements are fulfilled by the image of the stripe rather than the stripe itself. A few illustrative examples are given in Fig. 8: The contribution of the quartets  $(a;b)$  and  $(b;c)$ , for instance, is obtained from the products  $p_{58}$  and  $p_{811}$ , respectively. The quartet  $(a;c)$ , on the other hand, should not be introduced into expression (59) for via the product  $p_{511}$ . The distance from  $a$  to the image  $c^0$  is smaller than to  $c$  and so the quartet should be identified as either  $(a;c^0)$  or as  $(a^0;c)$ . The latter is the correct choice because the center of the quartet  $(a^0;c)$  satisfies  $-L_p/2 \leq X_{a^0c} = \frac{X_{a^0} + X_c}{2} = 2 < +L_p/2$ , while the center of the quartet  $(a;c^0)$  falls outside the primitive cell. The contribution to the expression for  $\gamma$  of this pair is, thus, obtained from the product  $p_{1113}$ .

The nice feature of the above examples is that the arguments we used to reach our decisions about the correct way to handle the quartets have not been based on the precise coordinates of the pairs, but rather on the identity of

the stripes and their locations with respect to the center of the simulation cell. This means that the products  $\sum_p \sum_q$  reproduce the contribution of all the quartets corresponding to the relevant stripes. Individual decisions are necessary only for a small number of quartets, associated with the following cases:

The first case is related with quartets in which the number of stripes separating the pairs is equal to  $M$ , as in the case of the pairs b and d in Fig. 8 which are located, respectively, inside the eighth and the twelfth stripes ( $M = 4$  in the above example). The separation between the pairs b and d along the x axis is very close to  $L_p=2$ , and it is impossible to know (without checking the coordinates of the pairs) whether the pair d should be replaced by its periodic image  $d^0$  located in the fourth strips. In a homogeneous system about half of such pairs should be exchanged with their images, and so the best estimate for the contribution to expression (59) for arising from quartets including one pair inside the eighth stripe and the other inside the twelfth stripes is:  $0.5 ( \frac{1}{4} + \frac{1}{12} )$ .

Another case occurs when the stripes containing the two pairs are symmetric with respect to the center of the primitive cell and, in addition, the distance between them is larger than  $M$ . A typical example is the quartet (a;d) in Fig. 8, in which a is inside the fifth stripe and d is in the twelfth strips. In this case it is obvious that (a;d) has to be replaced by either (a; $d^0$ ) or by ( $a^0$ ;d), but the two are equally probable. Therefore, the contribution of such quartets is best estimated by:  $0.5 ( \frac{1}{4} + \frac{1}{12} )$ .

The above rules for correct summation over the different quartets can be summarized by the following compact formula for the third term in expression (59):

$$\sum_{p=1}^M \sum_{q=1}^M f_{p;q} ; \quad (A 3)$$

where the function  $f$  is given by

$$f_{p;q} = \begin{cases} 1 & \text{for } |p - q| = M - 1 \text{ and } 2M + 1 < p + q < 6M + 1 \\ 0.5 & \text{for } |p - q| = M \text{ and } 2M + 1 < p + q < 6M + 1 \\ 0.5 & \text{for } |p - q| = M - 1 \text{ and } p + q = 2N + 1 \\ 0.5 & \text{for } |p - q| = M - 1 \text{ and } p + q = 6N + 1 \\ 0 & \text{otherwise} \end{cases} ; \quad (A 4)$$

The value of  $\langle \dots \rangle$  obtained using the above expressions [Eqs.(A 3) and (A 4)] are not accurate since the contribution of some of the quartets is introduced in an approximated way. However, the fraction of such quartets and the resultant numerical error can be diminished by taking the limit  $N_s \rightarrow \infty$ . In our simulations we have used a set of five approximations with  $N_s = 4;6;8;12;24$ .

Another "trick" to speed up the calculation of  $\langle \dots \rangle$ : The third and fourth terms in expression (59) for  $\langle \dots \rangle$  depend on the coordinates of the particles. Therefore, several values for these quantities can be obtained from a single MC configuration by generating replicas of the original simulation cell. These replicas can be generated by shifting the position of the origin of axes, and using the "minimal image convention" to define a replicated primitive cell which is centered around the new origin. The computational effort required for the calculation of expression (59) in the replicas is substantially smaller than that required for the generation of new MC configuration. For one special set of replicas the calculation can be done with (almost) no additional effort at all: This set include the replicas generated when the origin is shifted by constant intervals  $x = L_p = N_s$  in the x direction (  $y = L_p = N_s$  in the y direction). Such shifts are computationally favorable because they lead to cyclic permutations of the stripes, but do not mix the pairs included in each one of them.

- 
- [1] J. Israelachvili, *Intermolecular and Surface Forces* (Academic Press, London, 1985).
- [2] C. Tanford, *The Hydrophobic Effect* (Wiley, New York, 1980).
- [3] Micelles, Membranes, Microemulsions, and Monolayers, eds. W. M. Gelbart, A. Ben-Shaul, and D. Roux (Springer-Verlag, New York, 1994).
- [4] B. Alberts, D. Bray, J. Lewis, M. Ra, K. Roberts, and J. D. Watson, *Molecular Biology of the Cell* (Garland, New York, 1989).
- [5] M. J. Rosen, *Surfactants and Interfacial Phenomena* (Wiley, New York, 1978).
- [6] S. A. Safran, *Statistical Thermodynamics of Surfaces, Interfaces, and Membranes* (Addison-Wesley, New York, 1994).
- [7] *Structure and Dynamics of Membranes*, eds. R. Lipowsky and E. Sackmann (Elsevier, Amsterdam, 1995).
- [8] R. B. Gennis, *Biomembranes: Molecular Structure and Function* (Springer, New York, 1989).
- [9] *Statistical Mechanics of Membranes and Surfaces*, Proceedings of the Fifth Jerusalem Winter School for Theoretical Physics, eds. D. R. Nelson, T. Piran and S. Weinberg (World Scientific, Singapore, 1989).
- [10] A. G. Petrov *The Lyotropic State of Matter: Molecular Physics and Living Matter Physics* (Gordon and Breach, Amsterdam, 1999).
- [11] G. Gompper and M. Schick, *Self-Assembling Amphiphilic Systems*, Vol. 16 in *Phase Transitions and Critical Phenomena*, eds. C. Domb and J. L. Lebowitz (Academic Press, London 1994).
- [12] W. Helfrich, *Z. Naturforsch.* 28c, 693 (1973).
- [13] J. H. Schulman and J. B. Montagne, *Ann. N. Y. Acad. Sci.* 92, 366 (1961).
- [14] P. G. De Gennes and C. Taupin, *J. Phys. Chem.* 86, 2294 (1982).
- [15] O. Farago and P. Pincus, submitted to *Eur. Phys. J. E.*
- [16] L. Miao, U. Seifert, M. Wortis, and H.-G. Dobereiner, *Phys. Rev. E* 49, 5389 (1994).
- [17] U. Seifert, *Adv. Phys.* 46, 13 (1997), and references therein.
- [18] M. Wortis, M. Jaric, and U. Seifert, *J. Mol. Liquids* 71, 195 (1997).
- [19] W. Helfrich and R. M. Servuss, *Nuovo Cimento D* 3, 137 (1984).
- [20] S. T. Milner and S. A. Safran, *Phys. Rev. A* 36, 4371 (1987).
- [21] U. Seifert, *Z. Physik B* 97, 299 (1995).
- [22] W. Helfrich, *Z. Naturforsch.* 33a, 305 (1978).
- [23] A. G. Petrov and I. Bivas, *Prog. Surf. Sci.* 16, 389 (1984).
- [24] I. Szleifer, D. Kramer, A. Ben-Shaul, W. M. Gelbart, and S. A. Safran, *J. Chem. Phys.* 92, 6800 (1990).
- [25] D. Andelman, in Ref. [7].
- [26] E. Chacon, A. M. Somosa, and P. Tarazona, *J. Chem. Phys.* 109, 2371 (1998).
- [27] M. Bergstrom, *J. Chem. Phys.* 118, 1440 (2003), and many references therein.
- [28] J. S. Rowlinson and B. Widom, *Molecular Theory of Capillarity* (Clarendon Press, Oxford, 1982).
- [29] P. Schofield and J. R. Henderson, *Proc. R. Soc. London A* 379, 231 (1982).
- [30] M. M. Kozlov and V. S. Markin, *J. Chem. Soc. Faraday Trans. II* 85, 261 (1989).
- [31] E. M. Blokhuis and D. Bedeaux, *Mol. Phys.* 80, 705 (1993).
- [32] A. Robledo and C. Varea, *Physica A* 231, 178 (1996).
- [33] S. M. Oversteegen, P. A. Bameveld, F. A. M. Leemakers, and J. Lyklema, *Phys. Chem. Chem. Phys.* 1, 4987 (1999).
- [34] J. S. Rowlinson, *J. Phys. Cond. Matt.* 6, A1 (1994).
- [35] A. E. van Giessen and E. M. Blokhuis, *J. Chem. Phys.* 116, 302 (2002).
- [36] E. M. Blokhuis and D. Bedeaux, *Physica A* 184, 42 (1992).
- [37] E. M. Blokhuis, J. Groenewold, and D. Bedeaux, *Mol. Phys.* 96, 42 (1999).
- [38] U. Seifert and R. Lipowsky, in Ref. [7].
- [39] D. R. Squire, A. C. Holt, and W. G. Hoover, *Physica (Amsterdam)* 42, 388 (1969).
- [40] M. Parrinello and A. Rahman, *J. Chem. Phys.* 76, 2662 (1982).
- [41] O. Farago and Y. Kantor, *Phys. Rev. E* 61, 2478 (2000).
- [42] O. Farago, Ph.D. Thesis, Tel Aviv University (2001).
- [43] J. G. Kirkwood and F. P. Bu, *J. Chem. Phys.* 17, 338 (1949).
- [44] T. G. Trizenberg and R. Zwanzig, *Phys. Rev. Lett.* 28, 1183 (1972).
- [45] M. Plischke and B. Bergersen, *Equilibrium Statistical Physics* (World Scientific, London, 1994).
- [46] P. M. Chaikin and T. C. Lubensky, *Principles of Condensed Matter Physics* (Cambridge University Press, Cambridge, 1995).
- [47] O. Farago, *J. Chem. Phys.* 119, 596 (2003).
- [48] L. D. Landau and E. M. Lifshitz, *Theory of Elasticity* (Pergamon Press, Oxford, 1986).
- [49] D. C. Wallace, in *Solid State Physics*, eds. H. Ehrenreich, F. Seitz and D. Turnbull (Academic, New York, 1970), Vol. 25, pp. 301.
- [50] E. Lindahl and O. Edholm, *J. Chem. Phys.* 113, 3883 (2000).
- [51] W. Cai, T. C. Lubensky, P. Nelson, and T. Powers, *J. Phys. II (Paris)* 4, 931 (1994).
- [52] We would like to remind the reader that, in general, the area of the reference state does not coincide with the Schulman area which is the energy ground state of the system. The surface pressure which must be applied to  $\propto$  the area of the surface at the reference state is nothing but the negative of the surface tension.

- [53] We do not argue that the coordinates of atoms deform *independently*, but rather use transformation (32) as a mapping between the configuration phase spaces of the reference and the deformed systems.
- [54] W. Helfrich, Z. Naturforsch. 29c, 510 (1974).
- [55] S. Svetina, M. Brumen, and B. Zeks, Stud. Biophys. 110, 177 (1985); S. Svetina and B. Zeks, Eur. Biophys. J. 17, 101 (1989).
- [56] A classical example is the discussion on elasticity of thin plates in Ref. [48] (which has inspired many other works), where the area-difference rather than the bending energy is calculated.
- [57] L. Peliti and S. Leibler, Phys. Rev. Lett. 54, 1690 (1985).
- [58] W. Helfrich, J. Phys. (France) 46, 1263 (1985).
- [59] D. Forster, Phys. Lett. A 114, 115 (1986).
- [60] H. Kleinert, Phys. Lett. A 114, 263 (1986)
- [61] W. Helfrich, Eur. Phys. J B 1, 481 (1998).
- [62] H. A. Pinnow and W. Helfrich, Eur. Phys. J E 3, 149 (2000).
- [63] Y. Nishiyama, Phys. Rev. E 66, 061907 (2002).

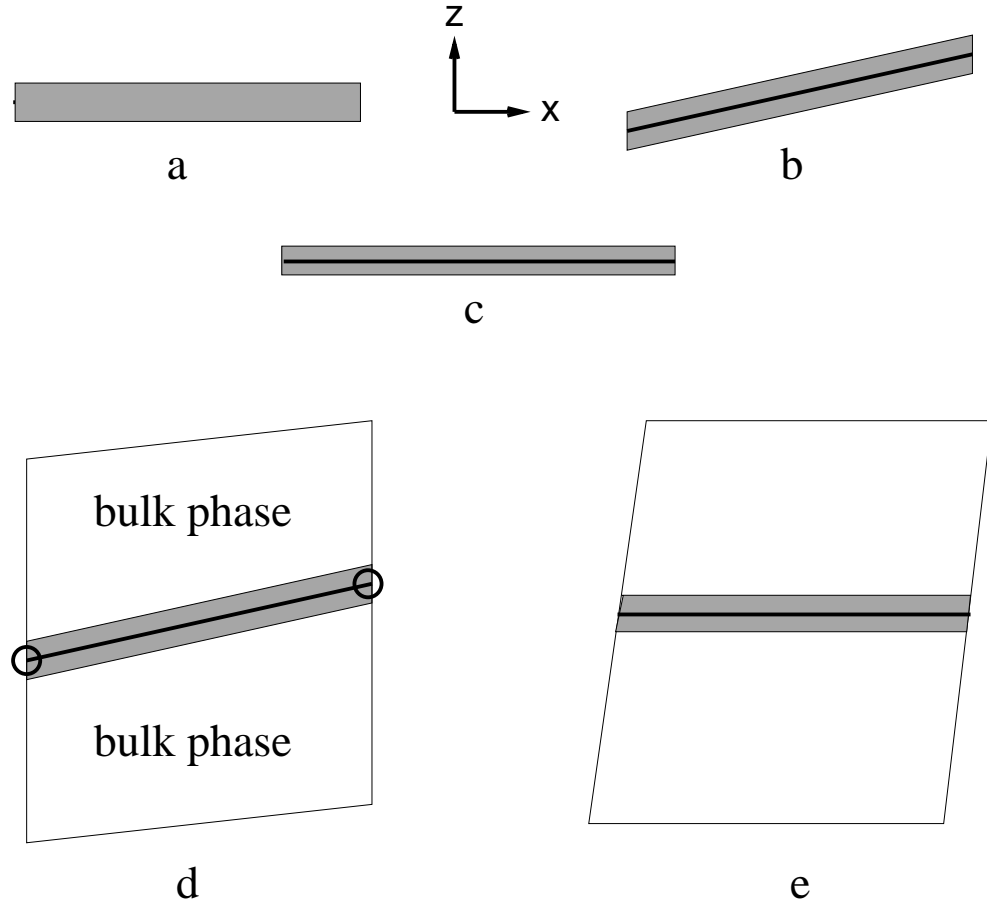


FIG . 1: A schematic picture of a bilayer membrane (gray) in the reference state (a), and in two deformed states (b) and (c). The solid line represents the characteristic surface of the membrane, to which the Helfrich free energy is applied. The areas of the characteristic surfaces and the volumes of the membranes (represented by the gray-shaded area in the figure) in (b) and (c) are identical. The membrane depicted in (b) is shown in (d) together with the containing cell and the embedding solvent. The end points marked by the open circles belong to the perimeter  $P$  of the characteristic surface. A another deformation of the container, which do not change the total area of the characteristic surface, is shown in (e).

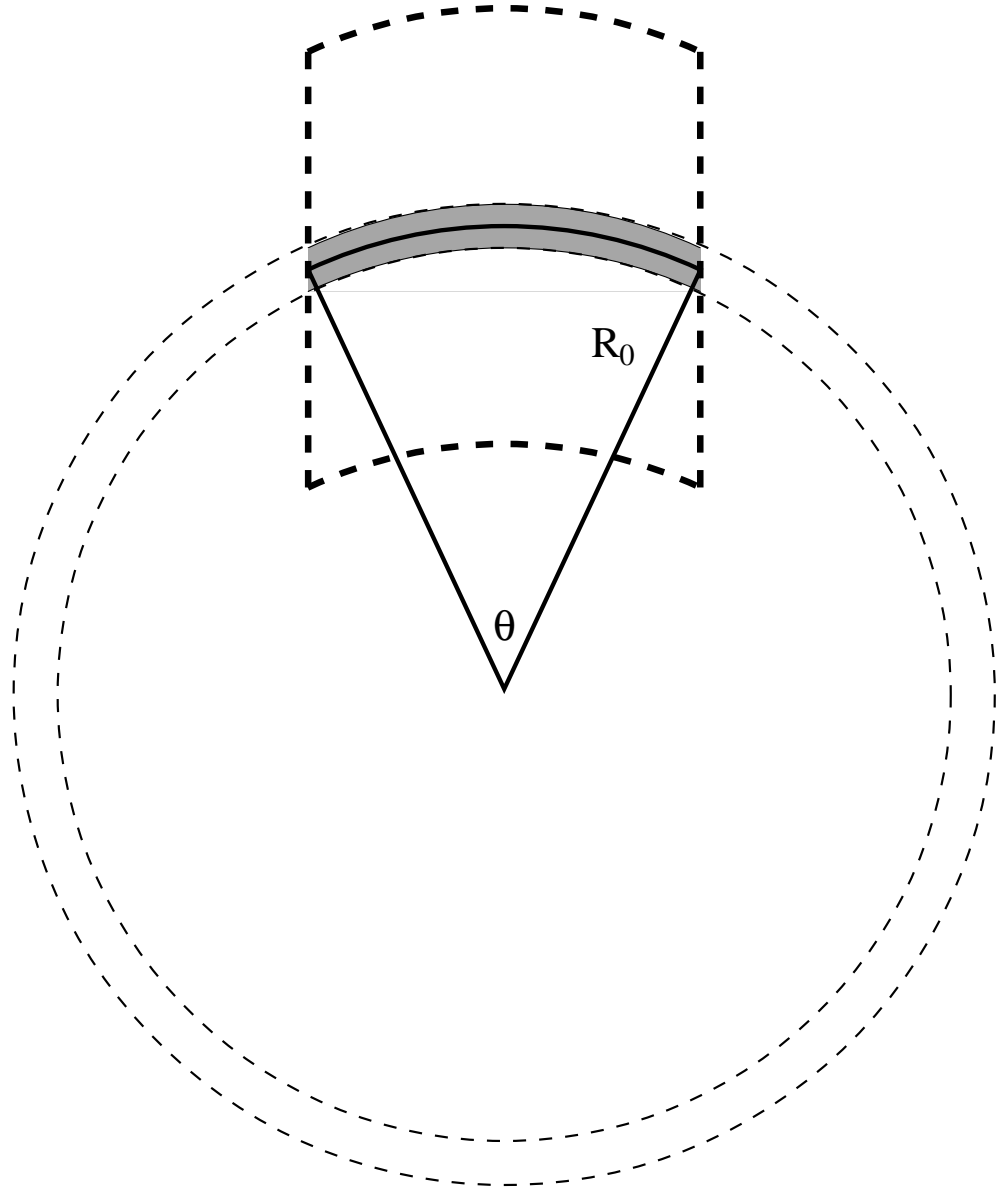


FIG. 2: A cylindrical bilayer membrane (gray) with radius of curvature  $R_0$  and apex angle  $\theta$ . The solid line in the middle of the membrane represents the characteristic surface. The cylindrical shape of the membrane is obtained via a deformation of the containing cell, depicted by the bold dashed line in the figure. The membrane may be thought of as part of a cylindrical vesicle (depicted by the thin dashed line) of a similar radius of curvature.

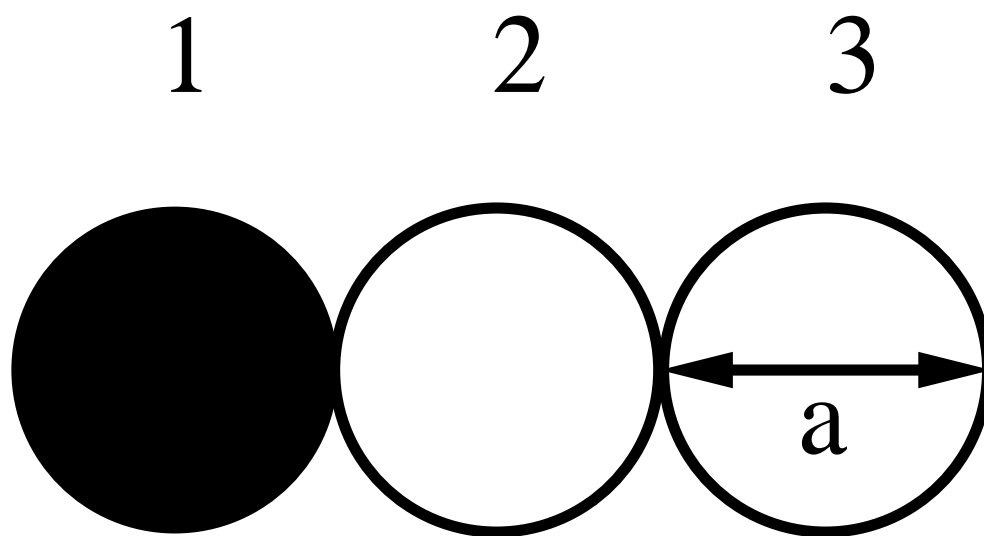


FIG. 3: A schematic picture of a lipid molecule in our model system – a trimer consisting of three spherical atoms of diameter  $a$ . The atom labeled 1 (solid circle) represents the hydrophilic head of the lipid, while the atoms labeled 2 and 3 (open circles) represent the hydrophobic tail.

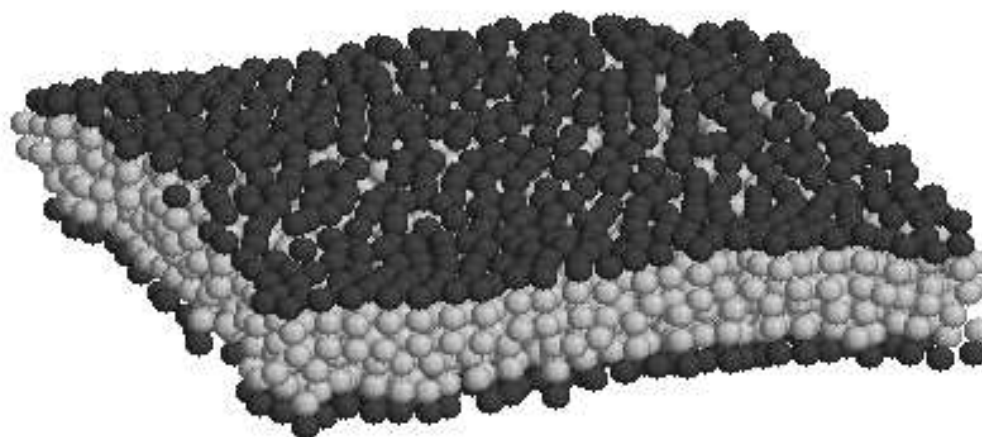


FIG. 4: Equilibrium configuration of a lipid membrane consisting of 1000 molecules (500 molecules in each monolayer).



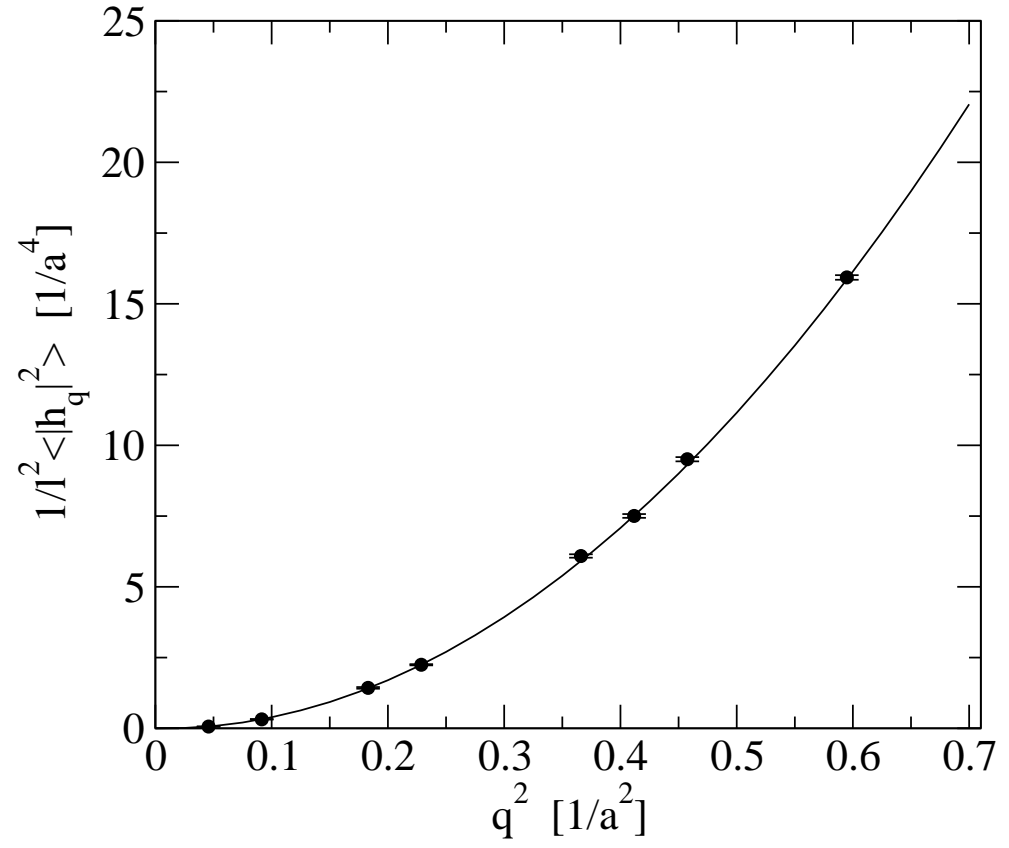


FIG. 5: The inverse of the spectral intensity for undulatory modes  $1/I^2 \langle |h_q|^2 \rangle$  as a function of the square wave number  $q^2$ . The circles mark numerical results, while the solid line depicts Eq.(75) with the values of  $\alpha$  and  $\beta$  given by Eq.(76)

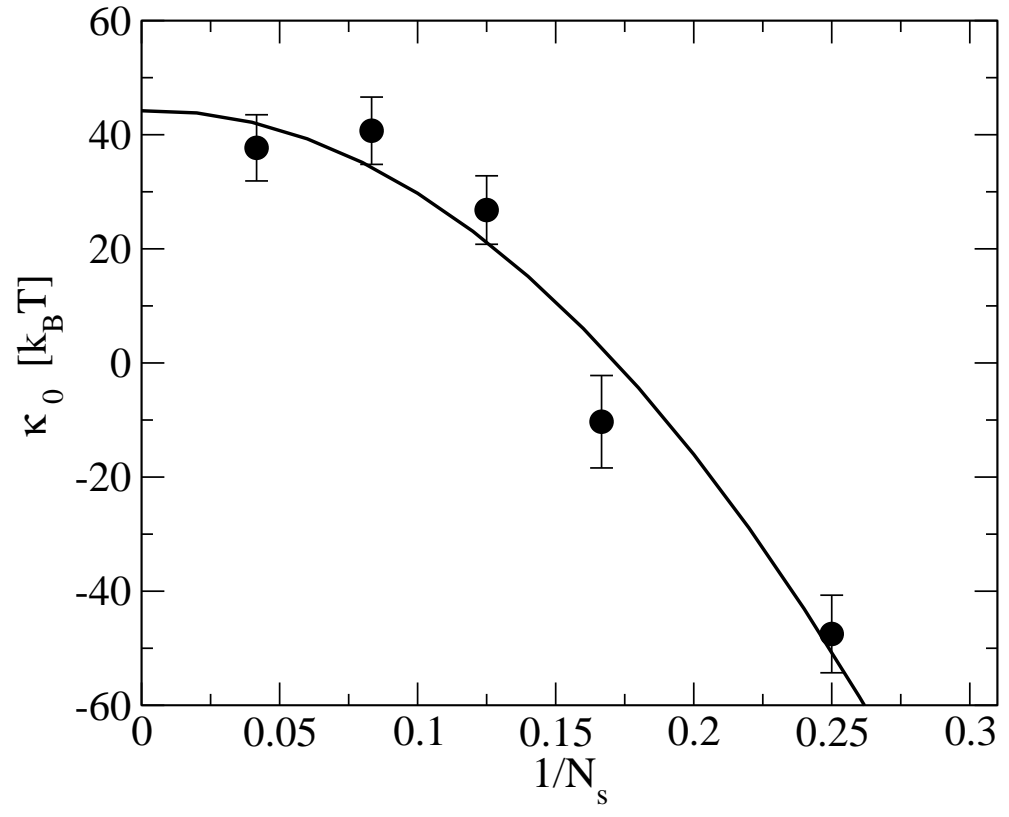


FIG .6: The bending modulus  $\kappa_0$  as a function of the inverse of number of stripes dividing the simulation cell,  $1/N_s$ . The curve depicts the weighted least square fit of a second order polynomial in  $1/N_s$  to the data.

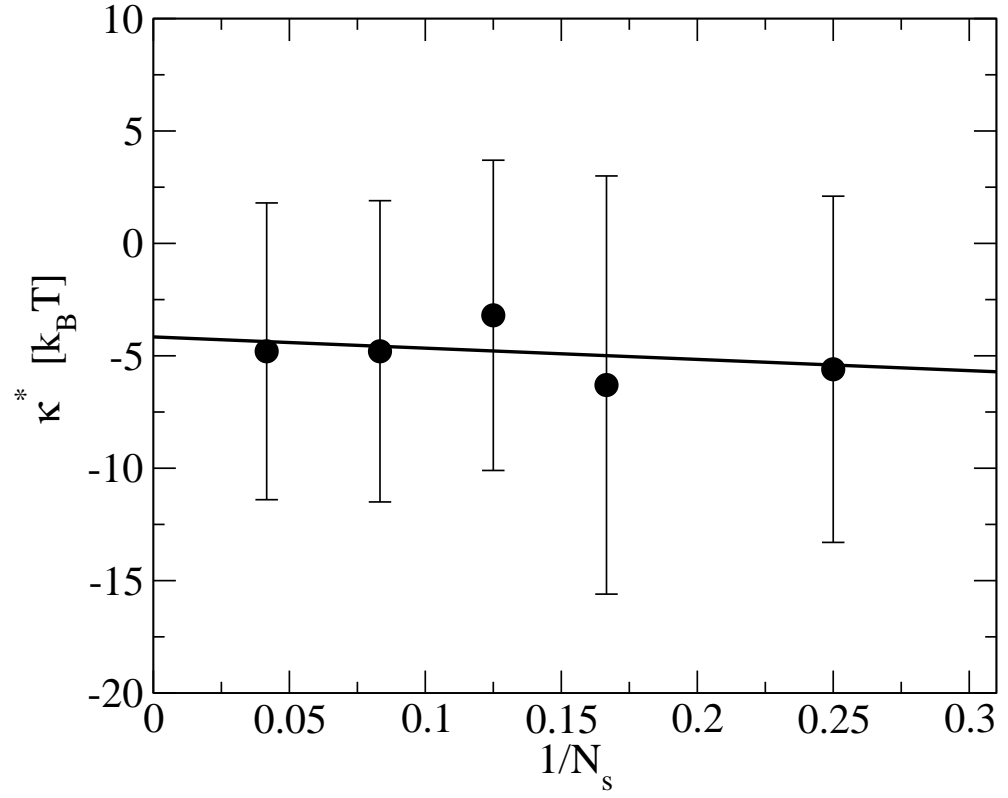


FIG. 7: The "apparent" bending modulus  $\kappa^*$  as a function of the inverse of number of stripes dividing the simulation cell,  $1/N_s$ . The curve depicts the weighted least square fit of a first order (linear) polynomial in  $1/N_s$  to the data.

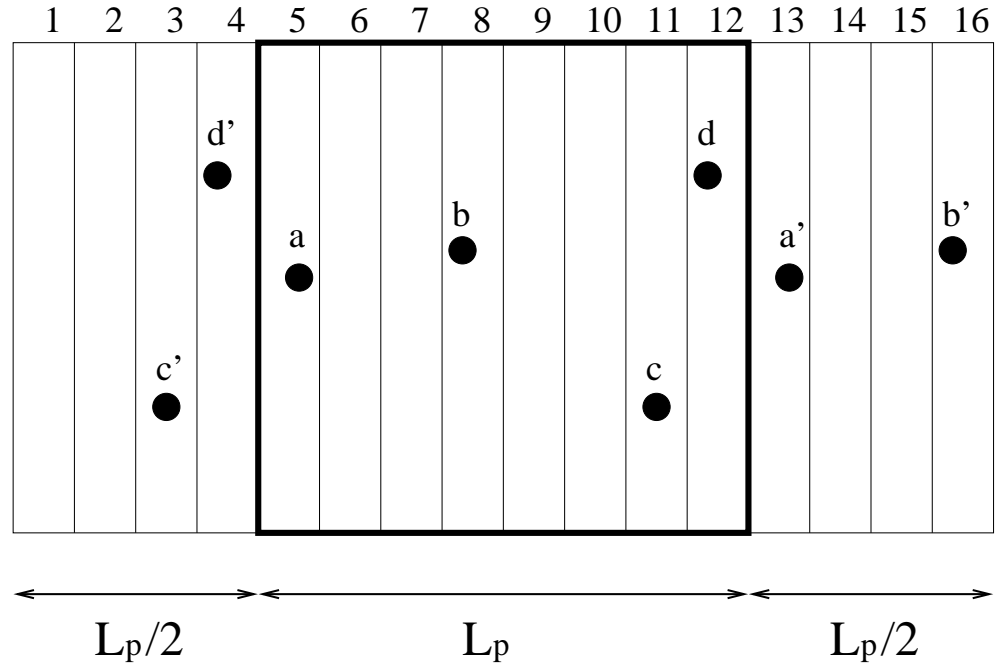


FIG. 8: A schematic picture of a system of linear size  $L_p$  consisting of four pairs ( $a, b, c, d$ ) and their periodic images ( $a', b', c', d'$ ). The bold frame marks the boundaries of the primitive simulation cell which is divided into  $N_s = 8$  stripes labeled from 5 to 12. The images of the stripes which belong to the nearest periodic extensions of the primitive cell are labeled 1-4 and 13-16.